Stem Cell Reports
Article

ISSCR

OPEN ACCESS

Restoration of hippocampal neural precursor function by ablation of senescent cells in the aging stem cell niche

Michael P. Fatt,[1,2] Lina M. Tran,[1,4] Gisella Vetere,[1] Mekayla A. Storer,[1] Jaclin V. Simonetta,[1,3] Freda D. Miller,[1,2,3,4,6,7,*] Paul W. Frankland,[1,2,4,5,*] and David R. Kaplan[1,2,3,*]

[1]Program in Neurosciences and Mental Health, Hospital for Sick Children, 18-9716 PGCRL, 686 Bay Street, Toronto, ON M5G 0A4, Canada
[2]Institute of Medical Science, University of Toronto, Toronto, ON M5S 1A8, Canada
[3]Department of Molecular Genetics, University of Toronto, Toronto, ON M5S 1A8, Canada
[4]Department of Physiology, University of Toronto, Toronto, ON M5S 1A8, Canada
[5]Department of Psychology, University of Toronto, Toronto, ON M5S 1A8, Canada
[6]Michael Smith Laboratories, University of British Columbia, Vancouver, BC V6T 1Z4, Canada
[7]Department of Medical Genetics, University of British Columbia, Vancouver, BC V6T 1Z4, Canada
*Correspondence: freda.miller@msl.ubc.ca (F.D.M.), paul.frankland@sickkids.ca (P.W.F.), dkaplan@sickkids.ca (D.R.K.)
https://doi.org/10.1016/j.stemcr.2021.12.010

SUMMARY

Senescent cells are responsible, in part, for tissue decline during aging. Here, we focused on CNS neural precursor cells (NPCs) to ask if this is because senescent cells in stem cell niches impair precursor-mediated tissue maintenance. We demonstrate an aging-dependent accumulation of senescent cells, largely senescent NPCs, within the hippocampal stem cell niche coincident with declining adult neurogenesis. Pharmacological ablation of senescent cells via acute systemic administration of the senolytic drug ABT-263 (Navitoclax) caused a rapid increase in NPC proliferation and neurogenesis. Genetic ablation of senescent cells similarly activated hippocampal NPCs. This acute burst of neurogenesis had long-term effects in middle-aged mice. One month post-ABT-263, adult-born hippocampal neuron numbers increased and hippocampus-dependent spatial memory was enhanced. These data support a model where senescent niche cells negatively influence neighboring non-senescent NPCs during aging, and ablation of these senescent cells partially restores neurogenesis and hippocampus-dependent cognition.

INTRODUCTION

Cellular senescence is one mechanism recently implicated in aging-induced tissue failure. Senescent cells accumulate in aging tissues and their pharmacological or genetic reduction rejuvenates aged tissues and extends lifespan (Baker et al., 2016; Chang et al., 2016; Childs et al., 2016; Roos et al., 2016). Senescent cells might also be important in neurodegeneration; senescent cells accumulate in the degenerating human brain, and clearance of these senescent cells in mouse models of neurodegeneration and obesity ameliorates some adverse sequelae (Musi et al., 2018; Bussian et al., 2018; Zhang et al., 2019; Ogrodnik et al., 2019, 2021). While these studies focused on senescent microglia, astrocytes, and oligodendrocyte progenitor cells, the adult brain contains many other cell types, including neural stem and precursor cells that generate new neurons important for cognition. Notably, in the hematopoietic system, stem cells are key targets for senescence-associated functional decline (Chang et al., 2016), suggesting that senescence of neural precursor cells (NPCs) and/or their surrounding niche cells may also negatively affect aging brain function. Indeed, increased expression of $P16^{INK4A}$, a cell-cycle regulator associated with senescence, causes decreased stem cell-mediated neurogenesis in aging mice (Micheli et al., 2019; Molofsky et al., 2006).

NPCs reside in two main regions of the mammalian brain, the subgranular zone (SGZ) of the hippocampal dentate gyrus (DG) and the ventricular-subventricular zone (V-SVZ) surrounding the lateral ventricles (Ming and Song, 2011). The hippocampal NPCs make dentate granule neurons that are important for memory formation and consolidation (Deng et al., 2010), while the V-SVZ NPCs make olfactory bulb interneurons that contribute to scent discrimination and olfactory learning (Moreno et al., 2009). Notably, hippocampal neurogenesis declines rapidly with age (Ben Abdallah et al., 2010; Walter et al., 2011), coincident with reduced stem cell activity (Walter et al., 2011; Ahlenius et al., 2009; Martín-Suárez et al., 2019) and decreased hippocampus-dependent cognitive function (Martinez-Canabal et al., 2019). Several mechanisms have been implicated in this age-associated neurogenic decline (Beckervordersandforth et al., 2017; Encinas et al., 2011; Mira et al., 2010; Seib et al., 2013; Villeda et al., 2011), but the underlying causes are still not clear. Here, we ask if cellular senescence is important in this context and show that senescent cells, predominantly NPCs, accumulate in the hippocampal SGZ niche and that these senescent cells negatively affect neurogenesis and hippocampus-dependent cognition, perturbations that can be partially reversed upon ablation of senescent cells.

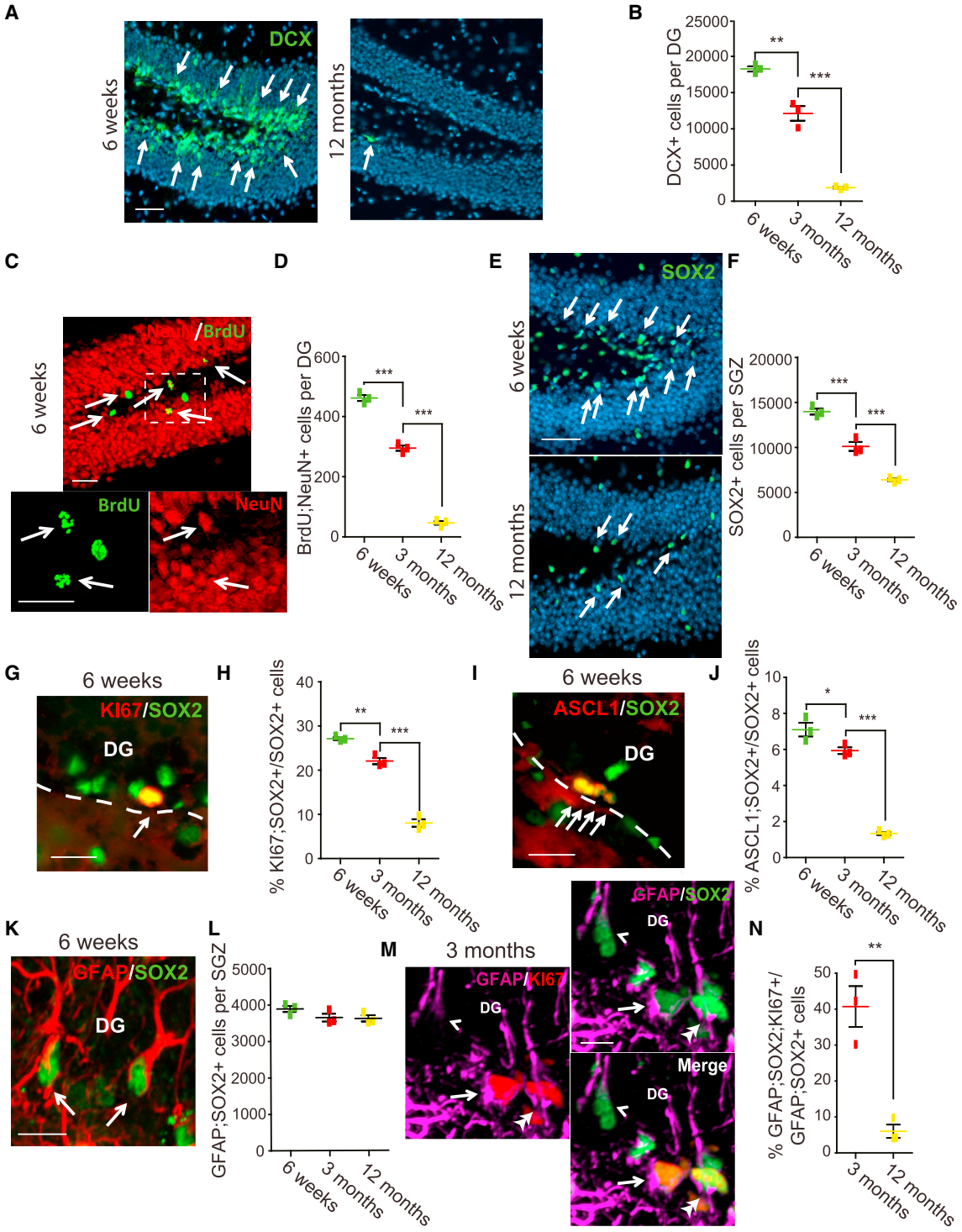

Figure 1. Hippocampal neurogenesis and precursor number decline during aging

Also see Figure S1. Coronal DG sections from 6 week, 3 month, and 12 month old mice were analyzed by immunostaining.

(A and B) Sections were immunostained for DCX (A, green, arrows), and total DG DCX-positive cells were quantified (B).

(C) DG image from a BrdU-injected 6 week mouse analyzed 1 month later, immunostained for BrdU (green) and NeuN (red). White hatched box is shown at higher magnification at the bottom. Arrows denote double-positive cells.

(D) Quantification of sections as in (C) for total DG BrdU-positive, NeuN-positive neurons.

(legend continued on next page)

RESULTS

Hippocampal neurogenesis and precursor number are reduced during murine aging

We used two approaches to characterize the previously reported aging-dependent decline in murine hippocampal neurogenesis from 6 weeks to 12 months (Ben-Abdallah et al., 2010; Walter et al., 2011). First, we immunostained for the immature neuron protein DOUBLECORTIN (DCX) (Figure 1A). DCX-positive DG neurons decreased by about 50% and 90% from 6 weeks to 3 months and 12 months, respectively (Figure 1B) (6 weeks, 18,263.3 ± 363.8; 3 months, 12,113.3 ± 1,009.5; 12 months, 1,876.6 ± 133.7). Second, we injected mice with bromodeoxyuridine (BrdU) and 30 days later quantified adult-born DG neurons by immunostaining for BrdU and the mature neuron protein NeuN (Figure 1C). Relative to 6 weeks, by 3 and 12 months BrdU-positive, NeuN-positive granule neurons were reduced by about 35% and 90% (Figure 1D) (6 weeks, 461.7 ± 10.1; 3 months, 295 ± 8.7; 12 months, 46.7 ± 6.0). Thus, hippocampal neurogenesis declines rapidly with age.

We asked if the decreased neurogenesis coincided with changes in NPCs initially by immunostaining SGZ sections for the pan-precursor marker SOX2 and the proliferation marker KI67 (Figures 1E and 1G). Relative to 6 weeks, SOX2-positive SGZ cells were decreased by about 30% and 50% at 3 and 12 months, respectively (Figure 1F) (6 weeks, 13,976.7 ± 338.9; 3 months, 10,110 ± 493.4; 12 months, 6,386.7 ± 144.5). The proportion of SOX2-positive NPCs expressing KI67 was also reduced by almost 3-fold at 12 months (Figure 1H) (6 weeks, 27.2% ± 0.3%, 3 months, 22.1% ± 0.7%, 12 months, 8.1% ± 0.9%). Thus, NPC proliferation and numbers decreased with aging.

Adult SGZ SOX2-positive NPCs include both transit amplifying (TA) cells and stem cells. We characterized these two populations separately. Analysis of immunostained sections showed that SOX2-positive cells expressing the TA cell marker ASCL1 were decreased by approximately 80% between 6 weeks and 12 months (Figures 1I and 1J) (6 weeks, 7.1% ± 0.4%; 3 months, 5.9% ± 0.2%; 12 months, 1.3% ± 0.1%). By contrast, SGZ neural stem cells (NSCs) were not significantly changed, as indicated by immunostaining for two combinations that distinguish NSCs from astrocytes, GFAP and NESTIN (6 weeks, 5,616.7 ± 53.3; 3 months, 5,270 ± 205.2; 12 months, 4,880 ± 252.4) (Figures S1A and S1B) or GFAP and SOX2 (Figures 1K and 1L) (6 weeks, 3,890 ± 83.3; 3 months, 3,646.7 ± 107.3; 12 months, 3,620 ± 85.4). However, these NSCs were significantly less proliferative by 12 months, as indicated by triple labeling for GFAP, SOX2, and KI67 (Figures 1M and 1N) (3 months, 40.7% ± 5.7%: 12 months, 6.0% ± 1.8%). Thus, proliferation of NSCs, numbers of TA cells, and neurogenesis are all decreased in the aging SGZ.

Senescent NPCs accumulate in the hippocampal neurogenic niche during aging

We next asked if senescent cells accumulate in the aging SGZ by staining for a widely used senescence marker, senescence-associated β-galactosidase (SA-β-Gal; Figure 2A). Relative to 6 weeks, SA-β-Gal-positive SGZ cells were increased almost 3-fold at 12 months (Figure 2B) (6 weeks, 511.7 ± 7.3; 3 months, 740 ± 47.3; 12 months, 1,356.7 ± 47.5). We confirmed that, as predicted, these cells were non-proliferative by injecting 12 month old mice with ethynyldeoxyuridine (EdU) and analyzing SA-β-Gal and EdU 24 h later. No SA-β-Gal-positive SGZ cells were positive for EdU.

We asked if the SA-β-Gal-positive SGZ cells were NPCs by co-labeling for SOX2 (Figure 2C). At 3 and 12 months most SA-β-Gal cells were also SOX2 positive, and quantification at 12 months showed that of 1,840 ± 68.5 total SA-β-Gal-positive SGZ cells, 1,565.2 ± 81.4 were SOX2 positive (85%) (see Figure 5C). We asked about the remaining SA-β-Gal-positive cells by immunostaining for the astrocyte

(E and F) Sections were immunostained for SOX2 (E, green, arrows), and total SGZ SOX2-positive cells were quantified (F).
(G and H) DG sections from 6 week (G) and older mice were immunostained for SOX2 (G, green) and KI67 (G, red; arrow denotes double-labeled cell), and the percentage of SOX2-positive SGZ cells that were also KI67 positive was quantified (H). Dashed line indicates the SGZ/hilus border.
(I and J) DG sections of 6 weeks (I) and older mice were immunostained for SOX2 (I, green) and ASCL1 (I, red; arrows denote double-positive cells), and the percentage of SOX2-positive SGZ cells that were also ASCL1 positive was quantified (J). Dashed line indicates the SGZ/hilus border.
(K and L) DG sections of 6 week (K) and older mice were immunostained for SOX2 (K, green) and GFAP (K, red; arrows denote double-positive cells), and total SGZ GFAP-positive, SOX2-positive cells were quantified (L).
(M and N) Six week (M) and 12-month DG sections were immunostained for GFAP (M, magenta), SOX2 (M, green), and KI67 (M, red; the arrow indicates a triple-positive cell, the arrowhead a SOX2-positive, GFAP-positive cell, and the double arrowhead a SOX2-positive, KI67-positive, GFAP-negative cell), and the percentage of GFAP-positive, SOX2-positive SGZ cells that were also KI67 positive was determined (N). In all cases, error bars indicate standard error of the mean (SEM), n = 3 mice/time point, and *p < 0.05, **p < 0.01, ***p < 0.001. Sections in (A and E) were counterstained for Hoechst 33258 (blue). Scale bars: 50 μm (A and E), 30 μm (C), 20 μm (G and I), and 10 μm (K and M).

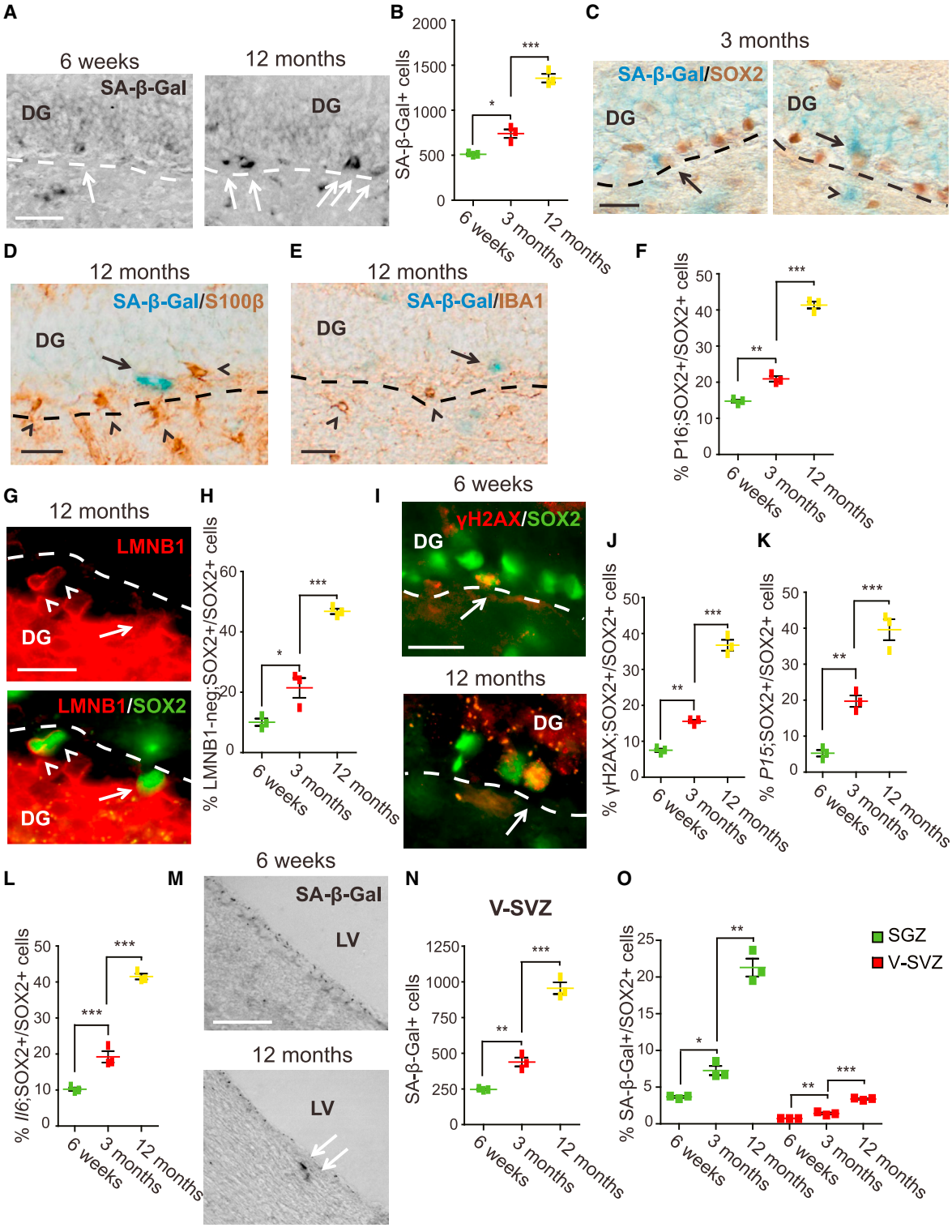

Figure 2. Senescent NPCs accumulate in the SGZ with age

Also see Figure S1. Coronal DG and V-SVZ sections from 6 week, 3 month, and 12 month old mice were analyzed histologically. (A and B) DG sections were stained for SA-β-Gal (A, black; arrows denote positive cells in the bright-field images), and total SGZ SA-β-Gal-positive cells were quantified (B). Dashed lines indicate the hilus/SGZ border.

(legend continued on next page)

marker S100β and the microglial marker IBA1 (Figures 2D and 2E). Quantification of double-labeled sections showed that at 12 months 15.3% of SA-β-Gal-positive cells expressed S100β (281.6 ± 12.2) and 6.4% IBA1 (118 ± 18.3) (see Figure 5C).

To confirm these findings, we analyzed hippocampal sections for three additional hallmarks of senescent cells, high expression of $P16^{INK4A}$ (He and Sharpless, 2017), loss of the tightly localized nuclear envelope protein LAMIN B1 (Freund et al., 2012), and accumulation of DNA damage, as indicated by γH2AX (Rodier et al., 2011). To detect $P16^{INK4A}$, we immunostained with a previously validated antibody (Kim et al., 2019); SOX2-positive, $P16^{INK4A}$-positive cells were increased almost 3-fold between 6 weeks and 12 months (Figure 2F; Figure S1C) (6 weeks, 14.8% ± 0.4%; 3 months, 20.9% ± 0.8%; 12 months, 41.4% ± 0.9%). A similar analysis for LAMIN B1 (Figure 2G) showed that at 6 weeks almost all SOX2-positive cells exhibited bright perinuclear LAMIN B1 immunoreactivity, but that by 12 months almost 50% of SOX2-positive cells were perinuclear LAMIN B1 negative (Figure 2H) (6 weeks, 10.1% ± 1.2%; 3 months, 21.5% ± 3.3%; 12 months, 46.8% ± 0.9%). We obtained similar results analyzing SOX2-positive cells with γH2AX-positive nuclear foci. These increased from 8% to 37% between 6 weeks and 12 months (Figures 2I and 2J) (6 weeks, 7.5% ± 0.4%; 3 months, 15.6% ± 0.4%; 12 months, 36.7% ± 1.5%). These increased percentages reflected an increase in total senescent NPCs with age. SOX2-positive, $P16^{INK4A}$-positive cells increased from 2,216.3 ± 76.2 to 2,642.0 ± 60.1 from 3 to 12 months; SOX2-positive, LAMIN B1-negative cells from 2,169.9 ± 331.6 to 2.990.0 ± 58.3; and SOX2-positive, γH2AX-positive cells from 1,573.8 ± 43.8 to 2,348.1 ± 97.0.

As final confirmation that SGZ NPCs senesce with age, we combined SOX2 immunostaining with single-molecule fluorescence *in situ* hybridization (FISH) for the senescence-associated mRNAs *P15ink4b* and *Il6* (Figures S1D and S1E). SOX2-positive NPCs expressing these two mRNAs significantly increased from 6 weeks to 12 months (Figures 2K and 2L) (*P15*—6 weeks, 5.3% ± 0.9%; 3 months, 19.7% ± 1.6%; 12 months, 39.6% ± 2.9%; *Il6*—6 weeks, 10.2% ± 0.4%; 3 months, 19.2% ± 1.6%; 12 months, 41.5% ± 0.8%). Thus, at 12 months, about 35%–40% of SOX2-positive SGZ NPCs are senescent.

We also asked about the V-SVZ, where neurogenesis does not decline as rapidly as in the SGZ (for example, see Shook et al., 2012). SA-β-Gal staining of forebrain lateral ventricle sections showed that senescent V-SVZ cells increased with age (Figures 2M and 2N) (6 weeks, 246.7 ± 4.4; 3 months, 438.3 ± 30.6; 12 months, 955 ± 40.1). However, when normalized to total SOX2-positive NPCs, the relative proportion of SA-β-Gal-positive cells was approximately 7-fold lower in the V-SVZ than in the SGZ at 12 months (Figure 2O) (SGZ—6 weeks, 3.7% ± 0.1%; 3 months, 7.4% ± 0.6%; 12 months, 21.3% ± 1.2%; V-SVZ—6 weeks, 0.72% ± 0.01%; 3 months, 1.4% ± 0.13%; 12 months, 3.38% ± 0.09).

Treatment with the senolytic agent ABT-263 reduces senescent NPCs in culture and *in vivo*

To ask about the biological importance of the senescent SGZ cells, we used the senolytic agent ABT-263 (Navitoclax), which induces apoptosis of various types of senescent cells (Bussian et al., 2018; Chang et al., 2016; Childs et al., 2016; Pan et al., 2017; Zhu et al., 2015). We asked if ABT-263 was also senolytic for NPCs by establishing a system for inducing NPC senescence. We cultured V-SVZ NPCs from 6 week old mice as neurospheres, passaged them, and exposed the secondary neurospheres for 72 h to low levels of the DNA-damaging agent camptothecin,

(C–E) Images of the 3 (C) or 12 month (D and E) DG stained for SA-β-Gal (blue) and immunostained for SOX2 (C, brown), S100β (D, brown), or IBA1 (E, brown). In (C) arrows denote double-positive cells, and the arrowhead denotes an SA-β-Gal-only cell. In (D and E) arrows denote cells positive for only SA-β-Gal and the arrowheads those positive for only S100β (D) or IBA1 (E). Dashed lines denote the hilus/SGZ border.

(F) Quantification of DG sections for the percentage of SOX2-immunoreactive SGZ cells that also immunostained positive for P16INK4A (see Figure S1C).

(G and H) DG sections from 12 month (G) or younger mice were immunostained for SOX2 (G, green) and LAMIN B1 (LMNB1) (G, red; arrows indicate a SOX2-positive, LMNB1-negative cell, and arrowheads double-positive cells), and the percentage of SOX2-positive SGZ cells negative for LMNB1 was determined (H). Dashed lines indicate the SGZ/hilus border.

(I and J) DG sections were immunostained for SOX2 (I, green) and γH2AX (I, red; arrows denote double-positive cells), and the percentage of SOX2-positive SGZ cells positive for γH2AX was determined (J). Dashed lines indicate the SGZ/hilus border.

(K and L) Quantification of sections analyzed by immunostaining for SOX2 and FISH for *P15ink4b* (K) or *Il6* (L) mRNAs. Shown are percentages of SOX2-positive SGZ NPCs positive for the relevant mRNA (see Figures 1D and 1E).

(M and N) V-SVZ sections were stained for SA-β-Gal (M, black; arrows denote positive cells), and total V-SVZ SA-β-Gal-positive cells were quantified (N). LV, lateral ventricle.

(O) Quantification of total SA-β-Gal-positive SGZ or V-SVZ cells expressed as a percentage of total SOX2-positive cells at the same time point. In all cases, error bars indicate SEM, n = 3 mice/time point, and *p < 0.05, **p < 0.01, ***p < 0.001. Scale bars: 50 μm (A and M), 25 μm (C–E), 20 μm (G and I).

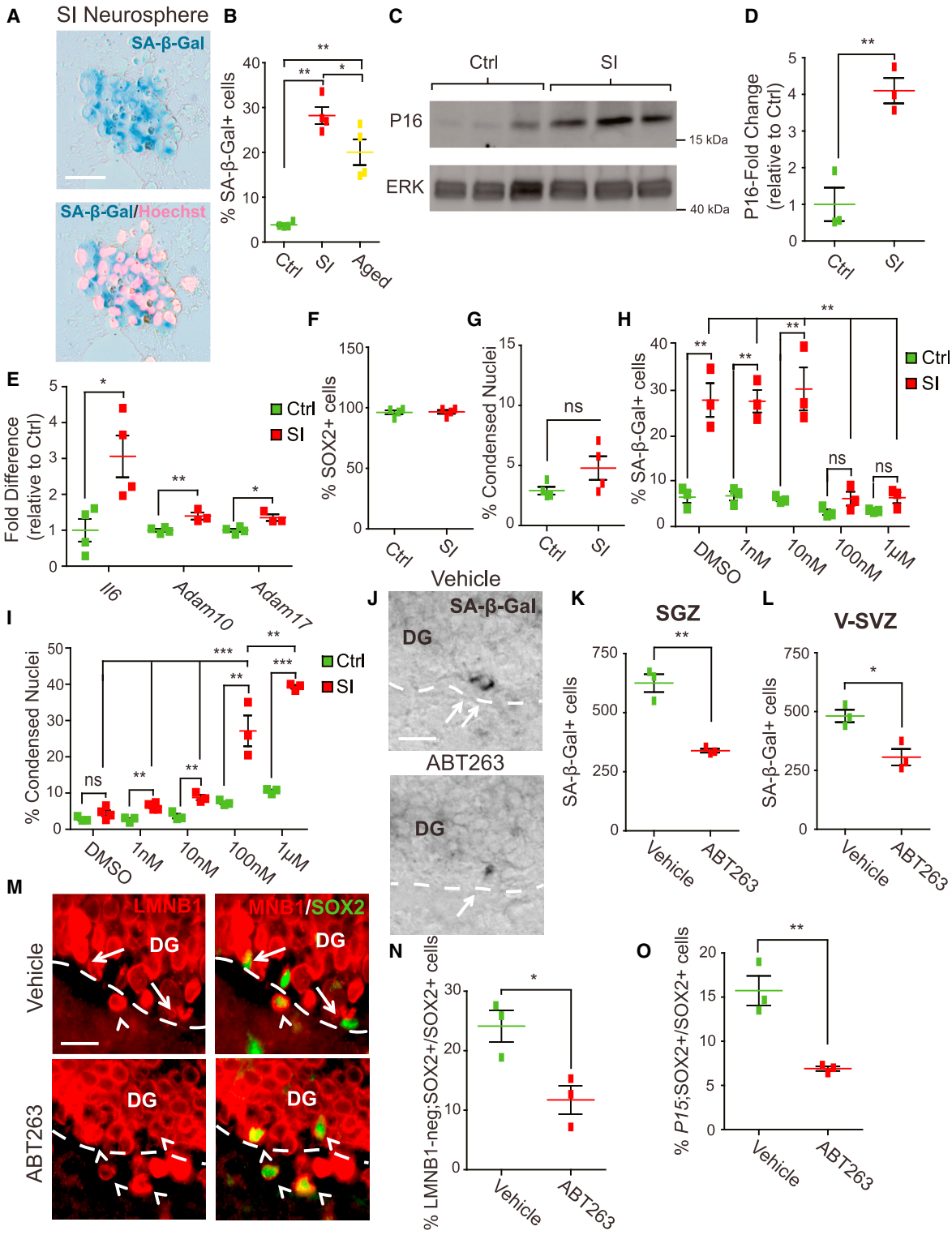

Figure 3. Administration of ABT-263 reduces senescent cells in the DG of young adult mice

(A–G) Primary neurospheres cultured from the 6 week V-SVZ were passaged, 2 days later treated for 72 h with 25 nM camptothecin (senescence-induced or SI) or vehicle (Ctrl), and characterized 2 days later.(A and B) Cultures were stained for SA-β-Gal (A, blue) and counterstained with Hoechst 33258 (pink), and the percentage of SA-β-Gal-positive cells was determined (B). For comparison, control

(legend continued on next page)

a treatment that causes senescence in other cell types (Han et al., 2002). Two days later, 3.8% ± 0.3% of vehicle-treated neurosphere cells were SA-β-Gal positive, as we reported previously (Fatt et al., 2014), and this was significantly increased to 28.2% ± 1.9% with camptothecin (Figures 3A and 3B). As a comparator, when neurospheres were cultured from the 20 month old V-SVZ, 20.0% ± 1.4% of the aged NPCs were SA-β-Gal positive (Figure 3B).

Two additional approaches confirmed this treatment-induced senescence. First, western blot analysis of similar cultures showed that $P16^{INK4A}$ levels were increased 4.1 ± 0.4-fold with camptothecin (Figures 3C and 3D). Second, quantitative PCR (qPCR) showed that three senescence-associated mRNAs, *Il6*, *Adam10*, and *Adam17* (Coppé et al., 2008; Kuilman et al., 2008), were also increased by camptothecin (Figure 3E) (*Il6*—control, 1.0 ± 0.31; camptothecin, 3.1 ± 0.58; *Adam10*—control, 1.0 ± 0.04; camptothecin, 1.4 ± 0.10; *Adam17*—control, 1.0 ± 0.05; camptothecin, 1.35 ± 0.9). Importantly, camptothecin did not alter the proportion of SOX2-positive neurosphere cells (Figure 3F), nor did it increase apoptotic cells with condensed or fragmented nuclei (Figure 3G) (control: 2.9% ± 0.32%; camptothecin, 4.8% ± 0.98%).

We then used this senescence culture system to ask about ABT-263. We treated neurospheres with camptothecin, replated them in fresh medium, added varying ABT-263 concentrations 24 h later, and stained for SA-β-Gal after an additional day. One and 10 nM ABT-263 had no effect on SA-β-Gal-positive cells in vehicle- or camptothecin-treated cultures (Figure 3H) (DMSO—control, 6.7% ± 0.28%; camptothecin, 28.5% ± 3.82%; 1 nM—control, 6.9% ± 1.05%; camptothecin, 28.3% ± 2.54%; 10 nM—control, 6.1% ± 0.39%; camptothecin, 31.0% ± 4.87%). However, at 100 nM and 1 μM, ABT-263 reduced SA-β-Gal-positive cells in camptothecin-treated cultures from 28% down to levels similar to vehicle-treated cultures (Figure 3H) (100 nM—control, 3.3% ± 0.63%; camptothecin plus ABT-263, 6.3% ± 0.78%; 1 μM—control, 3.5% ± 0.15%; camptothecin plus ABT-263, 6.5% ± 1.21%). To ask if ABT-263 was inducing apoptosis of senescent cells, as predicted, we quantified condensed, apoptotic nuclei. With 100 nM and 1 μM ABT-263, there were 27.2% ± 4.3% and 39.3% ± 0.5% apoptotic camptothecin-treated neurosphere cells compared with 7.3% ± 0.4% and 10.5% ± 0.4% apoptotic cells with vehicle treatment (Figure 3I). Thus, senescent NPCs were preferentially sensitive to the cytotoxic effects of ABT-263.

We next asked if ABT reduced senescent NPCs *in vivo*. We injected 3 month old mice intraperitoneally with 0.5 mg/kg ABT-263, a lower concentration than used in many other studies (Bussian et al., 2018; Chang et al., 2016). Analysis 5 days later showed that ABT-263 treatment decreased SA-β-Gal-positive SGZ cells by about 45% (Figures 3J and 3K) (vehicle, 625 ± 37.9; ABT-263, 339.2 ± 8.2) and SA-β-Gal-positive V-SVZ cells by about 35% (Figure 3L) (vehicle, 481.7 ± 26.2; ABT-263, 306.7 ± 34.9).

This ABT-263-mediated decrease in senescent SGZ NPCs was confirmed in two ways. First, immunostaining showed that ABT-263 caused a 50% reduction in the proportion of SOX2-positive SGZ cells that were negative for perinuclear LAMIN B1 (Figures 3M and 3N) (vehicle, 24.1% ± 2.7%; ABT-263, 11.7% ± 2.4%). Second, immunostaining and FISH showed that ABT-263 significantly decreased the proportion of SOX2-positive SGZ cells positive for the senescence-associated mRNA *P15ink4b* (Figure 3O) (vehicle, 15.7% ± 1.7%; ABT-263, 6.9% ± 0.3%). Thus, ABT-263 significantly reduced senescent NPCs in the adult hippocampus.

neurospheres from the 20 month old V-SVZ were also analyzed (B).(C and D) Western blots of SI or Ctrl neurospheres probed for $P16^{INK4A}$ (C, top) and reprobed for total ERK (bottom; molecular weight markers are shown to the right). $P16^{INK4A}$ levels were normalized to the ERK loading control and expressed as a fold change in SI versus Ctrl cultures (D).(E) qPCR of RNA isolated from SI or Ctrl neurospheres, analyzed for *Il6*, *Adam10*, or *Adam17* mRNAs. Values were normalized to *Gapdh* mRNA levels in the same samples and expressed as a fold change in SI versus Ctrl cultures.(F and G) Neurospheres were immunostained, counterstained with Hoechst 33258, and quantified for the percentage of SOX2-positive cells (F) and cells with condensed apoptotic nuclei (G).

(H and I) Cultures as in (A) were treated with varying ABT-263 concentrations for 24 h, stained, and analyzed for the percentages of cells that were SA-β-Gal-positive (H) or had condensed, apoptotic nuclei (I).

(J–O) Three month old mice were injected with ABT-263 or vehicle, and DG (J, K, M–O) or V-SVZ (L) sections were analyzed 5 days later.(J and K) DG sections were stained for SA-β-Gal (J, black; arrows denote positive cells), and total SGZ SA-β-Gal-positive cells were quantified (K). Dashed lines indicate the hilus/SGZ border.

(L) Quantification of stained V-SVZ sections for total SA-β-Gal-positive cells.(M and N) DG sections were immunostained for SOX2 (M, green) and LAMIN B1 (LMNB1) (red; arrows indicate SOX2-positive, LMNB1-negative cells, and arrowheads double-positive cells), and the percentage of SOX2-positive SGZ cells negative for LMNB1 was determined (N). Dashed lines indicate the SGZ/hilus border.(O) Sections were analyzed by immunostaining for SOX2 and FISH for *P15ink4b* mRNA and quantified for the percentage of SOX2-positive SGZ cells that were *P15ink4b* positive. In all cases, error bars indicate SEM. ns, not significant; *p < 0.05, **p < 0.01, ***p < 0.001.

In (B and D–I), n ≥ 3 independent cultures per condition. In (K, L, N, and O), n = 3 mice/condition. Scale bars: 20 μm.

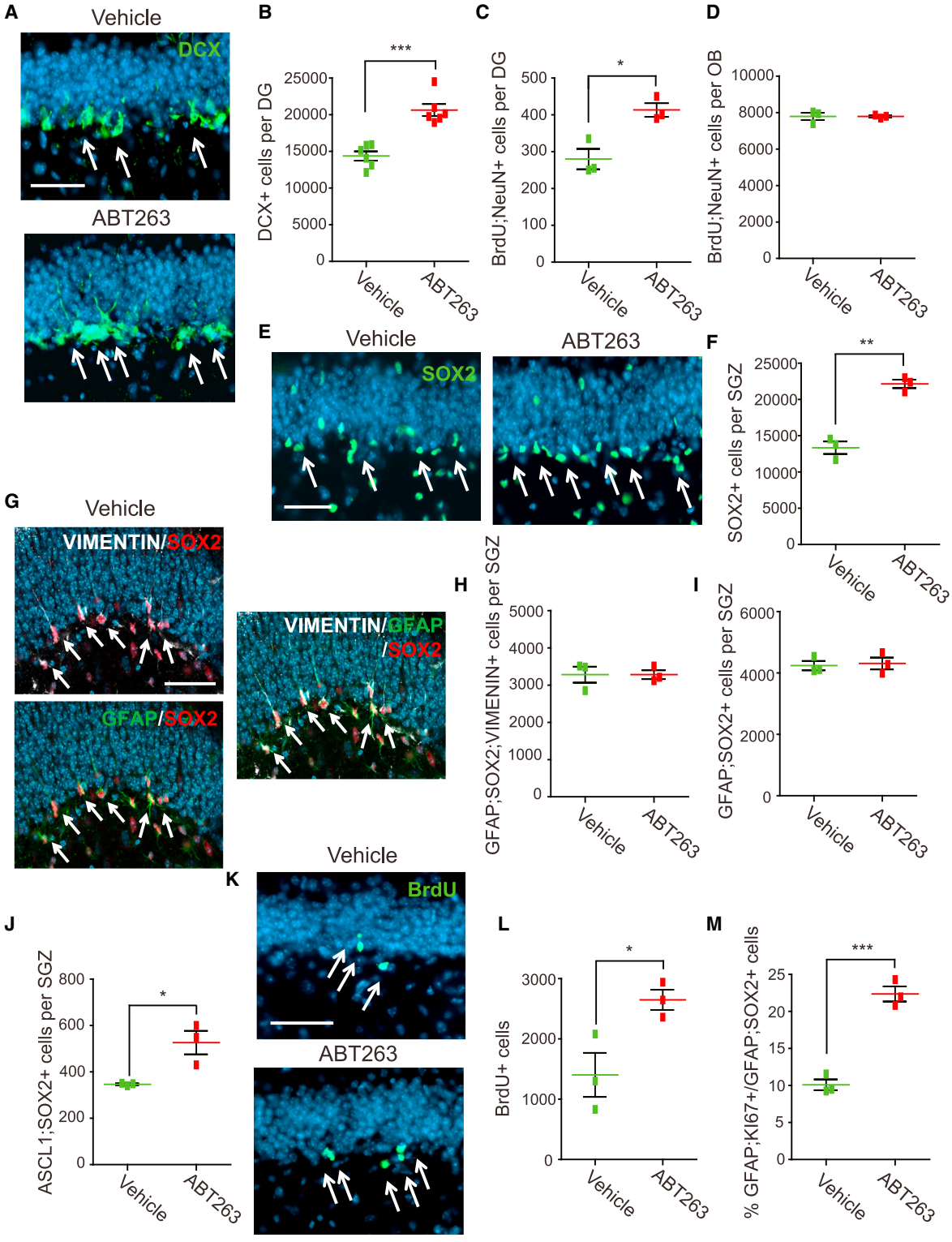

Figure 4. ABT-263 administration enhances hippocampal neurogenesis in adult mice

Also see Figure S2. Three month old mice were injected with ABT-263 or vehicle and sections were analyzed 5 days later. In (D and L) mice were also injected with BrdU 4 days post-ABT-263 and analyzed 24 h (L) or 30 days (D) later.

(A and B) Sections were immunostained for DCX (A, green, arrows), and total positive DG cells were quantified (B).

(legend continued on next page)

ABT-263-mediated ablation of senescent cells enhances adult hippocampal neurogenesis

We next asked if the ABT-263-mediated decrease in senescent cells in 3 month old mice affected SGZ neurogenesis using two approaches. First, we analyzed hippocampal sections 5 days following ABT-263 injection; immature DCX-positive neurons were increased almost 50% (Figures 4A and 4B; Figure S2) (vehicle, 14,376.7 ± 628.3; ABT-263, 20,641.7 ± 819.2). Second, we injected mice with vehicle or ABT-263 and 5 days later with BrdU, and then analyzed sections after a further 30 days. ABT-263 increased BrdU-positive, NeuN-positive adult-born dentate granule neurons by 48% (Figure 4C) (vehicle, 280 ± 27.5; ABT-263, 413.3 ± 18.6). By contrast, ABT-263 had no effect on V-SVZ neurogenesis, as measured by quantifying BrdU-positive, NeuN-positive olfactory bulb neurons in the same mice (Figure 4D) (vehicle, 7,785 ± 199.4; ABT-263, 7,786.7 ± 47.8).

We also analyzed SGZ NPCs following ABT-263 treatment. Immunostaining showed that SOX2-positive SGZ cells were increased 66% (Figures 4E and 4F) (vehicle, 13,353.3 ± 855.3; ABT-263, 22,150 ± 580.2). However, the number of SGZ NSCs was unaltered, as indicated by immunostaining for the NSC marker combinations SOX2, GFAP, and VIMENTIN (Figures 4G and 4H) (vehicle, 3,280 ± 215.2; ABT-263, 3,280 ± 117.9) or SOX2 and GFAP (Figure 4I) (vehicle, 4,240 ± 150.4; ABT-263, 4,310 ± 194.0). By contrast, SOX2-positive, ASCL1-positive TA cells were significantly increased (Figure 4J) (vehicle, 346.7 ± 3.4; ABT-263, 526.3 ± 50.4).

We also characterized NPC proliferation. Mice were injected with ABT-263 and 4 days later with BrdU, and the hippocampus was analyzed 24 h later. ABT-263 led to an 89% increase in BrdU-positive SGZ cells (Figures 4K and 4L) (vehicle, 1,403.3 ± 364.5; ABT-263, 2,648.3 ± 167.4). Moreover, GFAP-positive, KI67-positive SGZ NSCs were also increased by about 2-fold when normalized to total GFAP-positive, SOX2-positive SGZ cells (Figure 4M) (total GFAP-positive, KI67-positive cells—vehicle, 426.7 ± 40.4; ABT-263, 960.0 ± 17.3; proportion of proliferating NSCs—vehicle, 10.1% ± 0.7%: ABT-263, 22.4% ± 1.0%). Thus ABT-263 depletes senescent SGZ cells, and this results in enhanced proliferation of non-senescent NPCs and increased neurogenesis.

ABT-263-mediated ablation of senescent cells enhances hippocampal neurogenesis in 12 month old mice

We asked if senescent cell ablation had similar effects in older mice. We treated 12 month old mice with ABT-263 and 5 days later characterized senescent SGZ cells by SA-β-Gal staining (Figure 5A). ABT-263 decreased SA-β-Gal-positive cells by about 40% (Figure 5B) (vehicle, 1,513.3 ± 63.0; ABT-263, 938.3 ± 56.3), as observed at 3 months (Figure 3K). This decrease was almost entirely due to a decrease in senescent SOX2-positive NPCs as opposed to astrocytes or microglia, as indicated by co-labeling sections for SA-β-Gal and for SOX2, S100β, or IBA1 (Figure 5C) (SA-β-Gal cells—vehicle, 1,840 ± 68.5; ABT-263, 1,382 ± 108.1; $p < 0.01$; SA-β-Gal-positive, SOX2-positive NPCs—vehicle, 1,565.2 ± 81.4; ABT-263, 921.2 ± 57.5; SA-β-Gal-positive, S100β-positive astrocytes—vehicle, 281.6 ± 12.2; ABT-263, 265 ± 13.4; SA-β-Gal-positive, IBA1-positive microglia—vehicle. 118 ± 18.3; ABT-263, 93 ± 6.6). Consistent with this, the total numbers of IBA1-positive microglia were unaffected by ABT-263 treatment (Figures 5D and 5E) (vehicle, 1,566.7 ± 148.4; ABT-263, 1,596.7 ± 143.1).

We confirmed the SGZ senescent cell depletion using qRT-PCR to analyze *Il6* and *Mmp2* in RNA isolated from the 12 month DG 5 days post-treatment; both mRNAs were significantly decreased by ABT-263 (Figure 5F) (*Il6*—vehicle, 1.0 ± 0.07; ABT-263, 0.7 ± 0.10; $p < 0.05$; *Mmp2*—vehicle, 1.0 ± 0.11; ABT-263, 0.5 ± 0.10).

ABT-263 treatment also increased neurogenesis in the 12 month SGZ, as shown two ways. First, DCX-positive SGZ neurons were increased about 2.6-fold 5 days following ABT-263 treatment (Figure 5G) (vehicle, 1,150 ± 98.7; ABT-263, 3,046.7 ± 114.6). Second, BrdU-positive, NeuN-positive dentate granule neurons were also increased about 1.8-fold 35 days following ABT-263 treatment (BrdU

(C and D) Quantification of DG (C) or olfactory bulb (D) sections of ABT-263 or vehicle-treated mice injected with BrdU and analyzed 30 days later. Shown are total BrdU-positive, NeuN-positive cells.

(E and F) DG sections were immunostained for SOX2 (E, green, arrows), and total SGZ SOX2-positive cells were quantified (F).

(G and H) DG sections were immunostained for SOX2 (G, red), GFAP (G, green), and VIMENTIN (G, white), and total triple-positive SGZ cells (arrows) were quantified (H).

(I and J) Immunostained DG sections were quantified for total SOX2-positive SGZ cells that were also positive for GFAP (I) or ASCL1 (J).

(K and L) DG sections from mice injected with ABT-263/vehicle and then BrdU were immunostained 24 h post-BrdU to identify (K, green, arrows) and quantify (L) total BrdU-positive SGZ cells.

(M) Immunostained DG sections were analyzed for GFAP-positive, KI67-positive SGZ cells, and numbers were expressed as a percentage of total GFAP-positive, SOX2-positive SGZ cells as determined in (I). In all cases, error bars indicate SEM. $^{*}p < 0.05$, $^{**}p < 0.01$, $^{***}p < 0.001$. n = 3 mice/condition except in (B), where n = 6 mice/condition. In (A, E, G, and K) sections were counterstained with Hoechst 33258 (blue). Scale bars: 50 μm.

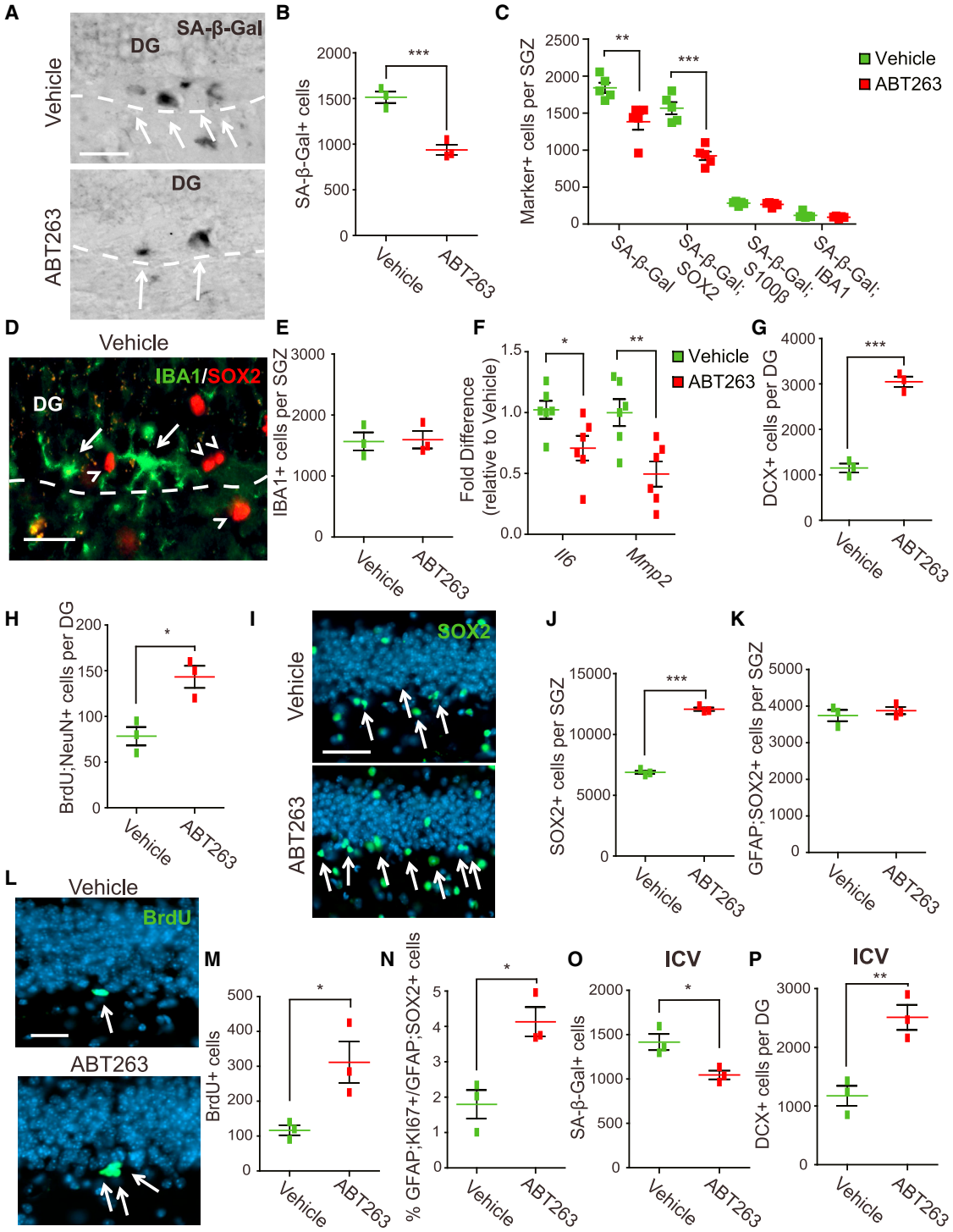

Figure 5. ABT-263 administration enhances neurogenesis and NPCs in 12 month old mice

(A–N) 12 month old mice were injected with ABT-263 or vehicle and the DG was analyzed 5 days later. In (H and M) mice were also injected with BrdU 4 days post-ABT-263 and analyzed 24 h (M) or 30 days (H) later. (A and B) DG sections were stained for SA-β-Gal (A, black, arrows), and total SA-β-Gal-positive SGZ cells were quantified (B). Dashed lines indicate the SGZ/hilus border. (C) DG sections were stained for SA-β-Gal and immunostained for SOX2, S100β, or IBA1 (as in Figures 2C–2E), and total SA-β-Gal-positive SGZ cells co-expressing each of these markers were quantified. Also quantified were total SA-β-Gal-positive cells. (D and E) DG sections were immunostained for SOX2

(legend continued on next page)

was injected 5 days after ABT-263) (Figure 5H) (vehicle, 78.3 ± 10.1; ABT-263, 143.3 ± 12.0).

We next analyzed NPCs in these ABT-treated aging mice. Immunostaining 5 days post-treatment showed that ABT-263 increased SOX2-positive SGZ cells by 76% (Figures 5I and 5J) (vehicle, 6,876.7 ± 134.8; ABT-263, 12,070 ± 141.1) without affecting the number of GFAP-positive, SOX2-positive NSCs (Figure 5K) (vehicle, 3,740 ± 153.9; ABT-263, 3,873.3 ± 97.7). We also asked about proliferation; mice were injected with ABT-263 and 4 days later with BrdU, and hippocampi were analyzed 24 h later. BrdU-positive SGZ cells were increased 2.7-fold (Figures 5L and 5M) (vehicle, 116.7 ± 14.5; ABT-263, 311.7 ± 59.3). This increase was due, in part, to NSCs, since GFAP-positive, KI67-positive SGZ cells were increased 2.3-fold when normalized to total GFAP-positive, SOX2-positive cells (Figure 5N) (vehicle, 1.8% ± 0.40; ABT-263, 4.1% ± 0.41).

Similar increases in NPC proliferation and hippocampal neurogenesis were seen when ABT-263 was directly injected into lateral ventricles of 12 month old mice. Analysis 5 days after intracerebroventricular (ICV) injection of ABT-263 showed that SA-β-Gal-positive SGZ cells were decreased (Figure 5O) (vehicle, 1,416.5 ± 91.2; ABT-263, 1,045 ± 49.3), while newborn DOUBLECORTIN-positive neurons were increased more than 2-fold (Figure 5P) (vehicle, 1,173.3 ± 170.7; ABT-263, 2,510 ± 214.6). Thus, ABT-263 pro-neurogenic effects can be mediated directly within the brain.

Genetic ablation of senescent cells in the aging SGZ increases NPC proliferation

Small molecules like ABT-263 can have off-target effects, so we also used a senescent-cell genetic-ablation approach, the P16-3MR mouse (Chang et al., 2016; Childs et al., 2016; Demaria et al., 2014). These mice carry a transgene wherein the *P16ink4a* promoter drives expression of thymidine kinase (TK) and mRFP; *P16ink4a*-positive senescent cells express this transgene and die when exposed to ganciclovir. Initially, we confirmed transgene expression in the aged SGZ by treating 12 month old mice with ABT-263 or vehicle, and performing qRT-PCR for *mRfp* mRNA in the DG 5 days later. *mRfp* mRNA was expressed and ABT-263-mediated senescent cell depletion caused a 4-fold decrease in its levels (Figure 6A) (vehicle, 1.00 ± 0.26; ABT-263, 0.24 ± 0.11).

We therefore treated 12 month old P16-3MR mice with either ganciclovir or PBS via continuous minipump-mediated infusion into the lateral ventricles for 7 days. Ganciclovir decreased SA-β-Gal-positive cells in the SGZ by approximately 33% (Figures 6B and 6C) (PBS, 1,515 ± 27.8; ganciclovir, 1,013.3 ± 23.3). Coincident with this, SOX2-positive SGZ cells were increased about 2-fold (Figures 6D and 6E) (PBS, 7,896.7 ± 127.3; ganciclovir, 13,400 ± 645.3), with no change in GFAP-positive, SOX2-positive NSCs (Figure 6F) (PBS, 3,893.3 ± 104.8; ganciclovir, 3,843.3 ± 64.9). To ask if NPC proliferation was increased, mice were also injected with BrdU on the sixth day of infusion. Relative to PBS, ganciclovir significantly increased both BrdU-positive SGZ cells (Figures 6G and 6H) (PBS, 183.3 ± 37.2; ganciclovir, 305 ± 23.1) and the ratio of GFAP-positive, KI67-positive SGZ cells to total GFAP-positive, SOX2-positive SGZ cells (Figure 6I) (PBS, 0.85% ± 0.16%: ganciclovir, 1.9% ± 0.29%). Thus, genetic ablation of senescent cells has the same effect on SGZ NPCs as does ABT-263.

Administration of ABT-263 to12 month old mice improves spatial memory

We next asked whether the ABT-263-induced increase in hippocampal neurogenesis was sufficient to enhance hippocampus-dependent spatial memory. We treated 12 month old mice with ABT-263 or vehicle, and 30 days later trained them (three trials per day for 6 days) to find a submerged platform in the Morris water maze. Both groups learned to locate the platform more efficiently across training (Figure 7A). One day following the training period, mice were evaluated in a probe test where the platform was removed, and the amount of time spent searching each zone was determined. Notably, compared with vehicle-treated mice, ABT-263-treated mice spent significantly more time

(D, red, arrowheads) and IBA1 (D, green, arrows), and total IBA1-positive SGZ cells were quantified (E). The dashed line indicates the hilus/SGZ border. (F) qPCR for *Il6* and *Mmp2* mRNAs in total DG mRNA. Values were normalized to *Gapdh* mRNA levels in the same samples and expressed as a fold change in ABT-263 versus vehicle-treated samples. (G) Quantification of immunostained sections for total DCX-positive cells in the DG. (H) Quantification of total BrdU-positive, NeuN-positive cells in the DG of ABT-263 or vehicle-treated mice injected with BrdU and analyzed 30 days later. (I and J) DG sections were immunostained for SOX2 (I, green, arrows), and total SGZ SOX2-positive cells were quantified (J). (K) Quantification of immunostained sections for total GFAP-positive, SOX2-positive SGZ cells. (L and M) DG sections from mice injected with ABT-263/vehicle and then BrdU were immunostained 24 h post-BrdU to identify (L, green, arrows) and quantify (M) total BrdU-positive SGZ cells. (N) Quantification of immunostained DG sections for GFAP-positive, KI67-positive SGZ cells, expressed as a percentage of total GFAP-positive, SOX2-positive SGZ cells as determined in (K).

(O and P) 12 month old mice were injected ICV with 50 ng of ABT-263 or vehicle, and coronal DG sections were analyzed 5 days later for total SA-β-Gal-positive SGZ cells (O) or total DCX-positive DG cells (P). In all cases, error bars indicate SEM. *$p < 0.05$, **$p < 0.01$, ***$p < 0.001$. n = 3 mice/condition in all cases, except for (C), where n = 5 mice/condition, and (F), where n = 6 mice/condition. Scale bars: 50 μm (A, I), 25 μm (D), 20 μm (L). In (I and L) sections were counterstained with Hoechst 33258 (blue).

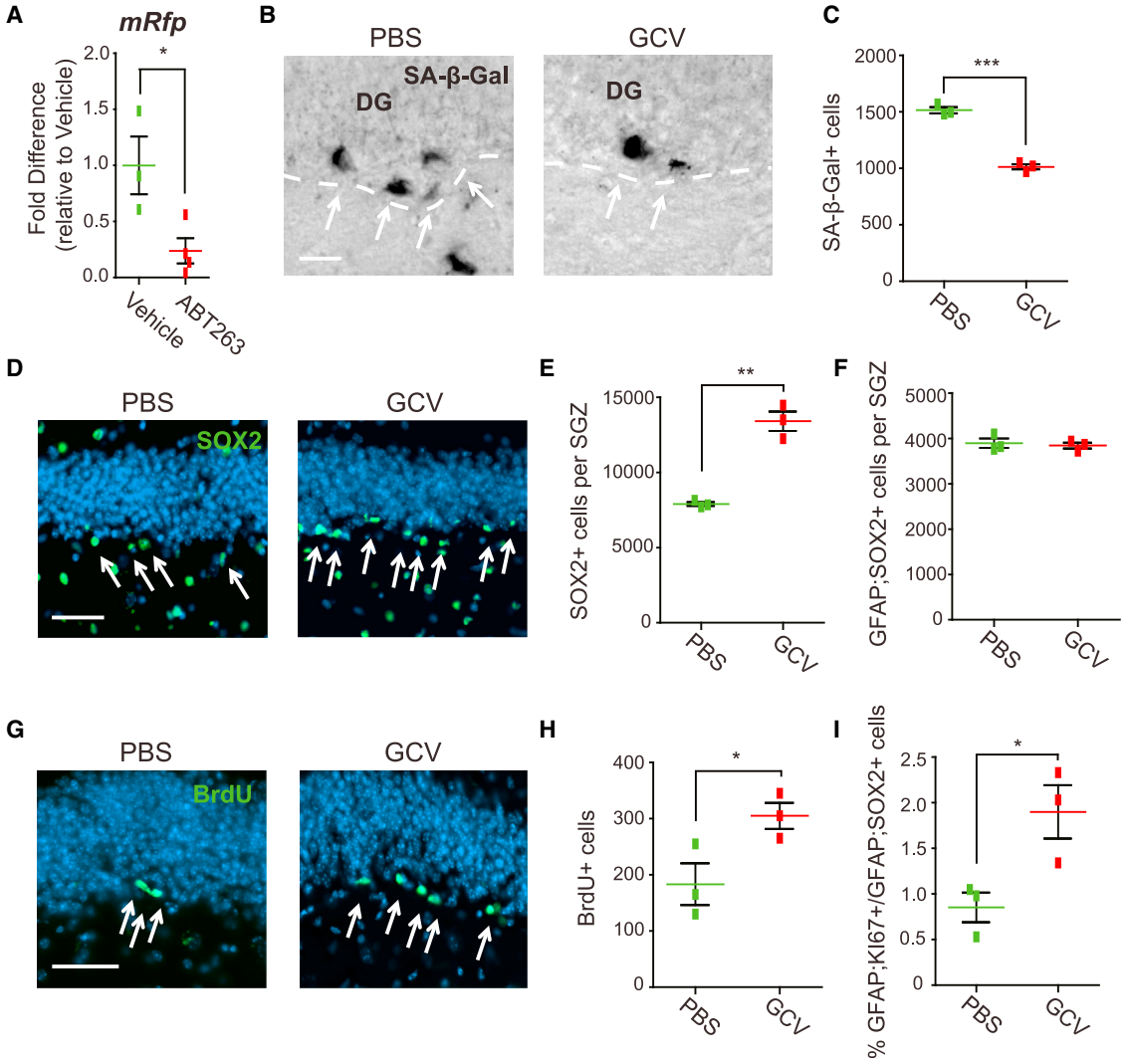

Figure 6. Genetic reduction of senescent cells in aged p16-3MR mice enhances hippocampal precursor proliferation and numbers

(A) qPCR for *mRfp* mRNA in total mRNA from the DG of 22 month old P16-3MR mice 5 days after intraperitoneal (i.p.) injection with ABT-263 or vehicle. Values are normalized to *Gapdh* mRNA in the same samples and expressed as a fold change relative to vehicle-injected mice.

(B–I) Twelve month old P16-3MR mice were infused ICV for 7 days with PBS or ganciclovir (GCV), and DG sections were analyzed. In (H) mice were also injected with BrdU after 6 days of infusion.

(B and C) DG sections were stained for SA-β-Gal (B, black, arrows), and total SA-β-Gal-positive SGZ cells were quantified (C). Dashed lines indicate the SGZ/hilus border.

(D and E) DG sections were immunostained for SOX2 (D, green, arrows), and total positive SGZ cells were quantified (E).

(F) Quantification of immunostained DG sections for total GFAP-positive, SOX2-positive SGZ cells.

(G and H) DG sections from mice injected with BrdU during GCV or PBS infusion were immunostained 24 h post-BrdU to identify (G, green, arrows) and quantify (H) total BrdU-positive SGZ cells.

(I) Quantification of immunostained DG sections for GFAP-positive, KI67-positive SGZ cells, expressed as a percentage of total GFAP-positive, SOX2-positive SGZ cells as determined in (F). In all cases, error bars indicate SEM and $n \geq 3$ mice/condition. In (D and G) sections were counterstained with Hoechst 33258 (blue). Scale bars: 20 μm (B) and 50 μm (D and G). *$p < 0.05$, **$p < 0.01$, ***$p < 0.001$.

searching in the target zone (Figures 7B and 7C) (vehicle—trained, 14.6% ± 3.3%; other, 8.9% ± 0.8%; $p < 0.05$; n = 14; ABT-263—trained, 21% ± 2.3%; other, 10.5% ± 1.2%; $p < 0.001$; n = 14; vehicle-trained versus ABT-263-trained, $p < 0.05$). Swim speed and total distance traveled were similar for both groups, indicating that general motor performance was not altered (Figures 7D and 7E) (swim speed—vehicle, 18.5 ± 0.6; ABT-263, 19.2 ± 0.5; distance

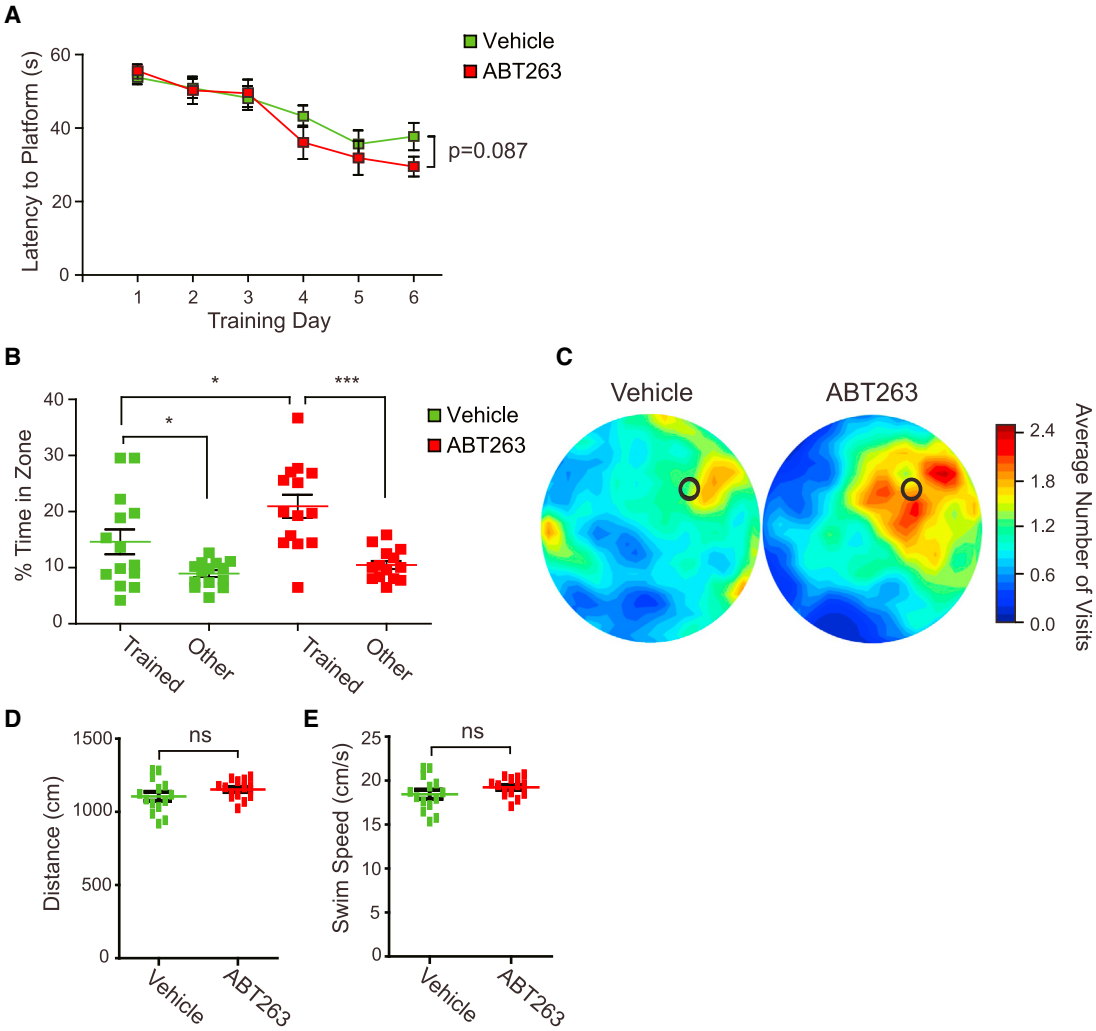

Figure 7. A single injection of ABT-263 enhances spatial memory in 12 month old mice

Twelve month old mice were treated with ABT-263 or vehicle and 30 days later were trained for 6 days on the hidden platform version of the Morris water maze.

(A) Average time to find the hidden platform on each day of training.

(B and C) Twenty-four hours following training, the platform was removed and a probe test performed to assess average amounts of time spent in the trained zone versus the other three equal-sized zones (B). Also shown are density plots of grouped data (C) showing where mice concentrated their searches, with the color scale representing average number of visits per mouse per 5 × 5 cm area. During training, the platform was located in the top right quadrant (C, black circle).

(D and E) Quantification of total distance traveled (D) and average swim speed (E) during the probe test. All results are representative of three independent experiments, and in all cases error bars indicate SEM. ns, not significant, $p > 0.05$; *$p < 0.05$; ***$p < 0.001$. n = 14 mice/condition.

traveled—vehicle, 1,106.0 ± 34.8; ABT-263, 1,152.9 ± 28.0; for both, $p > 0.05$; n = 14 per group). Thus, ABT-263 administration in middle-aged mice improves spatial learning and memory.

DISCUSSION

Our data show that the hippocampal neurogenic niche is subject to aging-induced senescence and that senescent SGZ cells, including senescent NPCs, interact with their non-senescent neighbors to reduce stem cell proliferation and neurogenesis. Our results provide further support for the notion that excessive senescence is a driving factor behind aging, and that midlife reduction of these cells can rejuvenate and restore the function of the stem cell niche. Collectively, these results indicate that senescent cells directly contribute to neurogenic decline in the middle-aged hippocampus, and that clearance of these cells

can partially restore hippocampal neurogenesis and function.

These data provide a potential explanation for the previously observed age-related decreases in hippocampal NPCs and neurogenesis (Ahlenius et al., 2009; Ben Abdallah et al., 2010; Walter et al., 2011) that we have confirmed here. Notably, we show that a substantive proportion of NPCs become senescent, thereby making them unavailable to generate new neurons, and that these senescent NPCs likely adversely affect neurogenesis from their non-senescent neighbors. Thus, our findings establish senescence, including NPC senescence, as one potential cause of neurogenic decline during aging.

This impairment could be caused by a decrease in the number of functional precursor cells (as we show here) that occurs as a consequence of genotoxic and ER stress, mitochondrial DNA damage, upregulation of cell-cycle inhibitors, and/or telomere erosion, all known to induce senescence. Alternatively, it could be due to niche degradation by secretion of scenescence-associated secretory phenotype (SASP) factors from senescent precursors themselves or other senescent niche cell types. In either case, when senescent cells in the niche are cleared, as we have done here, this could promote the rejuvenation and mobilization of the remaining normal stem cells, ultimately resulting in enhanced tissue function, maintenance, and repair.

We show that ABT-263 administration in middle-aged mice improves spatial learning and memory. The water maze paradigm used here is sensitive to perturbations of hippocampal neurogenesis in rodents. For example, interventions that suppress hippocampal neurogenesis impair spatial memory (Martinez-Canabal et al., 2019), whereas interventions that promote hippocampal neurogenesis improve spatial memory (Stone et al., 2011; Wang et al., 2012). One explanation for the ABT-263-mediated improvement in spatial learning and memory is that it is a consequence of the enhanced SGZ neurogenesis that occurs following the clearance of senescent cells. We cannot, however, rule out the possibility that systemic effects of ABT-263 or effects in regions other than the DG contributed to this improvement.

A potential role for cellular senescence in the brain has been most widely studied within the context of neurodegenerative disorders, with several publications reporting that senescent microglia, oligodendrocyte progenitor cells, and astrocytes are associated with neurodegenerative disorders, and that clearance of these senescent cells can rescue at least some of the adverse anatomical and behavioral sequelae in mouse models of these disorders (Bussian et al., 2018; Musi et al., 2018; Zhang et al., 2019, Ogrodnik et al., 2021). While these studies did not examine normal aging, it is possible that senescence of these other cell types could contribute to deregulating aging NPCs and inhibiting neurogenesis. This is particularly true for microglia and astrocytes, which are locally present within the hippocampal SGZ niche. However, our data show that senescent astrocytes and microglia together comprise only 21% of total senescent cells within the aging SGZ, and that ABT-263 treatment cleared 42% of senescent NPCs and only 12% of senescent astrocytes and microglia, arguing that the latter may play relatively minor roles in any local niche effects mediated by senescent cells. This specific effect of ABT-263 on NPCs and not microglia or astrocytes in the SGZ niche may be due to the lower concentrations of ABT-263 used in our experiments than in previous studies.

Our data show that aging has two distinct effects on SGZ stem cells. First, proliferation of NSCs was decreased, in part likely due to increased senescence. Second, the non-senescent NPCs that remained at 1 year of age were defective in their ability to proliferate and make neurons. We propose that senescent cells, including senescent NPCs, contribute to this latter effect since they can secrete SASP factors that reduce the proliferation and differentiation of their neighboring non-senescent precursor cells. Relevant to this, a report by Kalamakis et al. (2019) suggests that in the V-SVZ, an increase in pro-inflammatory signaling results in NSC quiescence and depletion during aging. We believe a similar mechanism governs age-dependent NSC quiescence/depletion in the SGZ, with senescent NPCs a major potential source of these quiescence-inducing factors, rather than a more generalized pro-inflammatory environment as described for the V-SVZ. In support of this idea, we found (data not shown) that camptothecin-treated and senescent cultured NPCs express SASP factors known to enforce the quiescence of other stem cell types, including IGFBP3 and SDF1. Ablation of even half of the senescent cells as we have done here would remove many of these deleterious SASP factors from the niche, thereby allowing NSCs to start to divide, resulting in a rapid restoration of precursor numbers and the generation of new neurons. This model is consistent with our data showing that one application of ABT-263 *in vivo* was sufficient to stimulate NPC proliferation after 5 days. The plethora of secreted SASP factors likely has multiple effects on the stem cell niche. Indeed, our data show that IL-6 is expressed by senescent SGZ NPCs, and we previously showed that excess IL-6 depletes the adult V-SVZ stem cell pool (Storer et al., 2018). Alternatively, SASP factors such as secreted matrix metalloproteinases (MMPs) might damage SGZ architecture, but it is unlikely that this type of structural damage could be reversed in such a short period of time.

Aging is associated with an increase in senescent cells that disrupt tissue structure and function (Gorgoulis et al., 2019). Safe-in-human senolytics such as ABT-263 (Navitoclax), developed for the treatment of cancer, are therefore

promising therapeutic agents to treat aging-associated conditions, with several in clinical trials to ablate senescent cells in osteoarthritis, diabetes complications, idiopathic pulmonary fibrosis, and chronic kidney disease (Robbins et al., 2021). Our findings suggest that senolytics may also be considered for age-related cognitive decline.

EXPERIMENTAL PROCEDURES

Animals

This study was approved by the Hospital for Sick Children Animal Care Committee, in accordance with Canadian Council on Animal Care guidelines. Wild-type C57BL/6J male and female mice ages 6 weeks and 3 months were obtained from The Jackson Laboratory. Twelve month old female mice were obtained as retired breeders (age approximately 7–9 months) and maintained in-house until the appropriate age. P16-3MR mice (Demaria et al., 2014) were generously provided by Unity Biotechnology (Brisbane, CA, USA), bred at the Hospital for Sick Children, and genotyped by standard PCR. For ABT-263 administration, mice were injected once intraperitoneally (i.p.) with 0.5 mg/kg ABT-263 (Selleck Chemicals, Houston, TX, USA) suspended in 45% PEG-400, 45% DDH_2O, and 10% DMSO. Some mice received 50 ng ABT-263 (suspended in 50% DMSO, 50% distilled H_2O) via ICV microinjection, as described below. For ganciclovir (GCV) administration, mice were implanted with ICV minipumps filled with a solution of 2.5 mg/mL GCV (Santa Cruz Biotechnology, Santa Cruz, CA, USA). For more details on ABT-263 and GCV administration, see the supplemental experimental procedures.

Neuroanatomy and immunostaining

Details are presented in the supplemental experimental procedures.

BrdU/EdU labeling

Details are presented in the supplemental experimental procedures.

Single molecule fluorescence *in situ* hybridization

Details are presented in the supplemental experimental procedures.

Water maze training and test probes

Mice were trained in the hidden platform version of the water maze. Details are presented in the supplemental experimental procedures. During training, we analyzed escape latency, distance traveled, and swim speed. In the probe test, we quantified spatial memory by measuring the amount of time the mice spent searching in the target zone (20 cm radius, centered on location of platform during training, corresponding to 11% of pool surface) versus average time spent in three other equivalent zones in other areas of the pool (Moser et al., 1998).

Western blots, qPCR, and neurosphere assays

Details are presented in the supplemental experimental procedures.

Quantification

Details are presented in the supplemental experimental procedures.

Statistics

Statistics were performed using the one-way ANOVA with Tukey's *post hoc* test or Student's unpaired t test to test for significance as appropriate and unless otherwise stated. For the drug treatment experiments, significance between the two treatment groups was determined using Student's paired t test, and significance across genotypes was determined with a two-way ANOVA with Tukey's *post hoc* test. All analyses were performed using Prism 5 (GraphPad, La Jolla, CA, USA). Significance was defined as $p < 0.05$.

SUPPLEMENTAL INFORMATION

Supplemental information can be found online at https://doi.org/10.1016/j.stemcr.2021.12.010.

AUTHOR CONTRIBUTIONS

M.P.F. conceptualized, performed, and analyzed most experiments and co-wrote the paper. L.N.T. and G.V., with P.W.F., conceptualized and performed the behavioral experiments. M.A.S. and J.V.S. performed some histochemical experiments and analyzed the results. F.D.M. and D.R.K. conceptualized experiments, analyzed data, and co-wrote the paper.

CONFLICTS OF INTEREST

The authors declare no competing interests.

ACKNOWLEDGMENTS

This work was funded by grants from the CIHR (MOP142267) and the CFREF "Medicine by Design" (CITA-2016-01) to F.D.M. and D.R.K. and by the CIHR (FDN143227) to P.W.F. We thank Judy Campisi for valuable discussions and advice and Remi Laberge, Yan Poon, and Unity Biotechnology for advice and informative discussions and supplying P16-3MR mice. We are very grateful to Patrik Ernfors for providing reagents and for hosting some of the experiments, and we thank Rebecca Parsons, Dennis Aquino, Sarah Burns, and Müge Altinkök for technical assistance.

Received: May 30, 2021
Revised: December 13, 2021
Accepted: December 14, 2021
Published: January 20, 2022

REFERENCES

Ahlenius, H., Visan, V., Kokaia, M., Lindvall, O., and Kokaia, Z. (2009). Neural stem and progenitor cells retain their potential for proliferation and differentiation into functional neurons despite lower number in aged brain. J. Neurosci. *29*, 4408–4419.

Baker, D.J., Childs, B.G., Durik, M., Wijers, M.E., Sieben, C.J., Zhong, J., Saltness, R.A., Jeganathan, K.B., Verzosa, G.C., Pezeshki, A., et al. (2016). Naturally occurring p16(Ink4a)-positive cells shorten healthy lifespan. Nature *530*, 184–189.

Beckervordersandforth, R., Ebert, B., Schäffner, I., Moss, J., Fiebig, C., Shin, J., Moore, D.L., Ghosh, L., Trinchero, M.F., Stockburger, C., et al. (2017). Role of mitochondrial metabolism in the control

of early lineage progression and aging phenotypes in adult hippocampal neurogenesis. Neuron *93*, 560–573.

Ben Abdallah, N.M.B., Slomianka, L., Vyssotski, A.L., and Lipp, H.P. (2010). Early age-related changes in adult hippocampal neurogenesis in C57 mice. Neurobiol. Aging *31*, 151–161.

Bussian, T.J., Aziz, A., Meyer, C.F., Swenson, B.L., van Deursen, J.M., and Baker, D.J. (2018). Clearance of senescent glial cells prevents tau-dependent pathology and cognitive decline. Nature *562*, 578–582.

Chang, J., Wang, Y., Shao, L., Laberge, R.M., Demaria, M., Campisi, J., Janakiraman, K., Sharpless, N.E., Ding, S., Feng, W., et al. (2016). Clearance of senescent cells by ABT263 rejuvenates aged hematopoietic stem cells in mice. Nat. Med. *22*, 78–83.

Childs, B.G., Baker, D.J., Wijshake, T., Conover, C.A., Campisi, J., and van Deursen., J.M. (2016). Senescent intimal foam cells are deleterious at all stages of atherosclerosis. Science *354*, 472–477.

Coppé, J.P., Patil, C.K., Rodier, F., Sun, Y., Muñoz, D.P., Goldstein, J., Nelson, P.S., Desprez, P.Y., and Campisi, J. (2008). Senescence-associated secretory phenotypes reveal cell-nonautonomous functions of oncogenic RAS and the p53 tumor suppressor. PLoS Biol. *6*, 2853–2868.

Demaria, M., Ohtani, N., Youssef, S.A., Rodier, D., Toussaint, W., Mitchell, J.R.,., Laberge, R.M., Vijg, J., Van Steeg, H., Dollé, M.E.T., et al. (2014). An essential role for senescent cells in optimal wound healing through secretion of PDGF-AA. Dev. Cell *31*, 722–733.

Deng, W., Aimone, J.B., and Gage, F.H. (2010). New neurons and new memories: how does adult hippocampal neurogenesis affect learning and memory? Nat. Rev. Neurosci. *11*, 339–350.

Encinas, J.M., Michurina, T.V., Peunova, N., Park, J.H., Tordo, J., Peterson, D.A., Fishell, G., Koulakov, A., and Enikolopov, G. (2011). Division-coupled astrocytic differentiation and age-related depletion of NSCs in the adult hippocampus. Cell Stem Cell *8*, 566–579.

Fatt, M.P., Cancino, G.I., Miller, F.D., and Kaplan, D.R. (2014). p63 and p73 coordinate p53 function to determine the balance between survival, cell death and senescence in adult neural precursor cells. Cell Death Differ. *21*, 1546–1559.

Freund, A., Laberge, R.M., Demaria, M., and Campisi, J. (2012). Lamin B1 loss is a senescence-associated biomarker. Mol. Biol. Cell *23*, 2066–2075.

Gorgoulis, V., Adams, P.D., Alimonti, A., Bennett, D.C., Bischof, O., Bishop, C., Campisi, J., Collado, M., Evangelou, K., Ferbeyre, G., et al. (2019). Cellular senescence: defining a path forward. Cell *179*, 813–827.

Han, Z., Wei, W., Dunaway, S., Darnowski, J.W., Calabresi, P., Sedivy, J., Hendrickson, E.A., Balan, K.V., Pantazis, P., and Wyche, J.H. (2002). Role of p21 in apoptosis and senescence of human colon cancer cells treated with camptothecin. J. Biol. Chem. *277*, 17154–17160.

He, S., and Sharpless, N.E. (2017). Senescence in health and disease. Cell *169*, 1000–1011.

Kalamakis, G., Brüne, D., Ravichandran, S., Bolz, J., Fan, W., Ziebell, F., Stiehl, T., Catalá-Martinez, F., Kupke, J., Zhao, S., et al. (2019). Quiescence modulates stem cell maintenance and regenerative capacity in the aging brain. Cell *176*, 407–1419.

Kim, H.N., Chang, J., Iyer, S., Han, L., Campisi, J., and Manolagas, S.C. (2019). Elimination of senescent osteoclast progenitors has no effect on the age-associated loss of bone mass in mice. Aging Cell *18*, e12923.

Kuilman, T., Michaloglou, C., Vredeveld, L.C., Douma, S., van Doorn, R., Desmet, C.J., Aarden, L.A., Mooi, W.J., and Peeper, D.S. (2008). Oncogene-induced senescence relayed by an interleukin-dependent inflammatory network. Cell *133*, 1019–1031.

Martinez-Canabal, A., Akers, K.G., Josselyn, S.A., and Frankland, P.W. (2019). Age-dependent effects of hippocampal neurogenesis suppression on spatial learning. Hippocampus *23*, 66–74.

Martín-Suárez, S., Valero, J., Muro-García, T., and Encinas, J.M. (2019). Phenotypical and functional heterogeneity of neural stem cells in the aged hippocampus. Aging Cell *18*, e12958.

Micheli, L., D'Andrea, G., Ceccarelli, M., Ferri, A., Scardigli, R., and Tirone, F. (2019). p16ink4a prevents the activation of aged quiescent DG stem cells by physical exercise. Front Cell Neurosci *13*, 10.

Ming, G., and Song, H. (2011). Adult neurogenesis in the mammalian brain: significant answers and significant questions. Neuron *70*, 687–702.

Mira, H., Andreu, Z., Suh, H., Lie, D.C., Jessberger, S., Consiglia, A., San Emeterio, J., Hortigüela, R., Marqués-Torrejón, M.A., Nakashima, K., et al. (2010). Signaling through BMPR-IA regulates quiescence and long term activity of NSCs in the adult hippocampus. Cell Stem Cell *7*, 78–89.

Molofsky, A.V., Slutsky, S.G., Moseph, N.M., He, S., Pardal, R., Krishnamurthy, J., Sharpless, N.E., and Morrison, S.J. (2006). Increasing p16INK4a expression decreases forebrain progenitors and neurogenesis during ageing. Nature *443*, 448–452.

Moreno, M.M., Linster, C., Escanilla, O., Sacquet, J., Didier, A., and Mandairon, N. (2009). Olfactory perceptual learning requires adult neurogenesis. Proc. Natl. Acad. Sci. U S A *106*, 17980–17985.

Moser, E.I., Krobert, K.A., Moser, M.B., and Morris, R.G. (1998). Impaired spatial learning after saturation of long-term potentiation. Science *281*, 2038–2042.

Musi, N., Valentine, J.M., Sickora, K.R., Baeuerle, E., Thompson, C.S., Shen, Q., and Orr, M.E. (2018). Tau protein aggregation is associated with cellular senescence in the brain. Aging Cell *17*, e12840.

Ogrodnik, M., Zhu, Y., Langhi, L.G.P., Tchkonia, T., Krüger, P., Fielder, E., Victorelli, S., Ruswhandi, R.A., Giorgadze, N., Pirtskhalava, T., et al. (2019). Obesity-induced cellular senescence drives anxiety and impaires neurogenesis. Cell Metab. *29*, 1061–1077.

Ogrodnik, M., Evans, S.A., Fielder, E., Victorelli, S., Kruger, P., Salmonowicz, H., Weigand, B.M., Patel, A.D., Pirtskhalava, T., Inman, C.L., et al. (2021). Whole-body senescent cell clearance alleviates age-related brain inflammation and cognitive impairment in mice. Aging Cell *20*, e13296.

Pan, J., Li, D., Xu, Y., Zhang, J., Wang, Y., Chen, M., Lin, S., Huang, L., Chung, E.J., Citrin, D.E., et al. (2017). Inhibition of Bcl2-xl with ABT-263 selectively kills senescent type II pneumocytes and reverses persistent pulmonary fibrosis induced by ionizing radiation in mice. Int. J. Radiat. Oncol. Biol. Phys. *99*, 353–361.

Robbins, P.D., Jurk, D., Khosla, S., Kirkland, J.L., LeBrasseur, N.K., Miller, J.D., Passos, J.F., Pignolo, R.J., Tchkonia, T., and

Niedernhofer, L.J. (2021). Senolytic drugs: reducing senescent cell viability to extend health span. Annu. Rev. Pharmacol. Toxicol. *61*, 779–803.

Rodier, F., Muñoz, D.P., Teachenor, R., Chu, V., Le, O., Bhaumik, D., Coppé, J.P., Campeau, E., Beauséjour, C.M., Kim, S.H., et al. (2011). DNA-SCARS: distinct nuclear structures that sustain damage-induced senescence growth arrest and inflammatory cytokine secretion. J. Cell Sci. *124*, 68–81.

Roos, C.M., Zhang, B., Palmer, A.K., Orgrodnik, M.B., Pirtskhalaba, T., Thalji, N.M., Hagler, M., Jurk, D., Smith, L.A., Casaclang-Verzosa, G., et al. (2016). Chronic senolytic treatment alleviates established vasomotor dysfunction in aged or atherosclerotic mice. Aging Cell *15*, 973–977.

Seib, D.R.M., Corsini, N.S., Ellwanger, K., Plaas, C., Mateos, A., Pitzer, C., Niehrs, C., Celikel, T., and Martin-Vallalba, A. (2013). Loss of Dickkopf-1 restores neurogenesis in old age and counteracts cognitive decline. Cell Stem Cell *12*, 204–214.

Shook, B.A., Manz, D.H., Peters, J.J., Kang, S., and Conover, J.C. (2012). Spatiotemporal changes to the subventricular zone stem cell pool through aging. J. Neurosci. *32*, 6947–6956.

Stone, S.S.D., Teixeira, C.M., DeVito, L.M., Zaslavsky, K., Josselyn, S.A., Lozano, A.M., and Frankland, P.W. (2011). Stimulation of entorhinal cortex promotes adult neurogenesis and facilitates spatial memory. J. Neurosci. *31*, 13469–13484.

Storer, M.A., Gallagher, D., Fatt, M.P., Simonetta, J.V., Kaplan, D.R., and Miller, F.D. (2018). Interleukin-6 regulates adult NSC numbers during normal and abnormal postnatal development. Stem Cell Rep. *10*, 1464–1480.

Villeda, S.A., Luo, J., Mosher, K.I., Zou, B., Britschgi, M., Bieri, G., Stan, T.M., Fainberg, N., Ding, Z., Eggel, A., et al. (2011). The aging systemic milieu negatively regulates neurogenesis and cognitive function. Nature *477*, 90–94.

Walter, J., Keiner, S., Witte, O.W., and Redecker, C. (2011). Age-related effects on hippocampal precursor cell subpopulations and neurogenesis. Neurobiol. Aging *32*, 1906–1914.

Wang, J., Gallagher, D., DeVito, L.M., Cancino, G.I., Tsui, D., He, L., Keller, G.M., Frankland, P.W., Kaplan, D.R., and Miller, F.D. (2012). Metformin activates an atypical aPKC-CBP pathway to promote neurogenesis and enhance spatial memory formation. Cell Stem Cell *11*, 23–35.

Zhang, P., Kishimoto, Y., Grammatikakis, I., Gottimukkala, K., Cutler, R.G., Zhang, S., Abdelmohsen, K., Bohr, V.A., Sen, J.M., Gorospe, M., and Mattson, M.P. (2019). Senolytic therapy alleviates Aβ-associated oligodendrocyte progenitor cell senescence and cognitive deficits in an Alzheimer's disease model. Nat. Neurosci. *22*, 719–728.

Zhu, Y., Tchkonia, T., Fuhrmann-Stroissnigg, H., Dai, H.M., Ling, Y.Y., Stout, M.B., Pirtskhalava, T., Giorgadze, N., Johnson, K.O., Giles, C.B., et al. (2015). Identification of a novel senolytic agent, navitoclax, targeting the Bcl-2 family of anti-apoptotic factors. Aging Cell *15*, 428–435.

Stem Cell Reports, Volume *17*

Supplemental Information

Restoration of hippocampal neural precursor function by ablation of senescent cells in the aging stem cell niche

Michael P. Fatt, Lina M. Tran, Gisella Vetere, Mekayla A. Storer, Jaclin V. Simonetta, Freda D. Miller, Paul W. Frankland, and David R. Kaplan

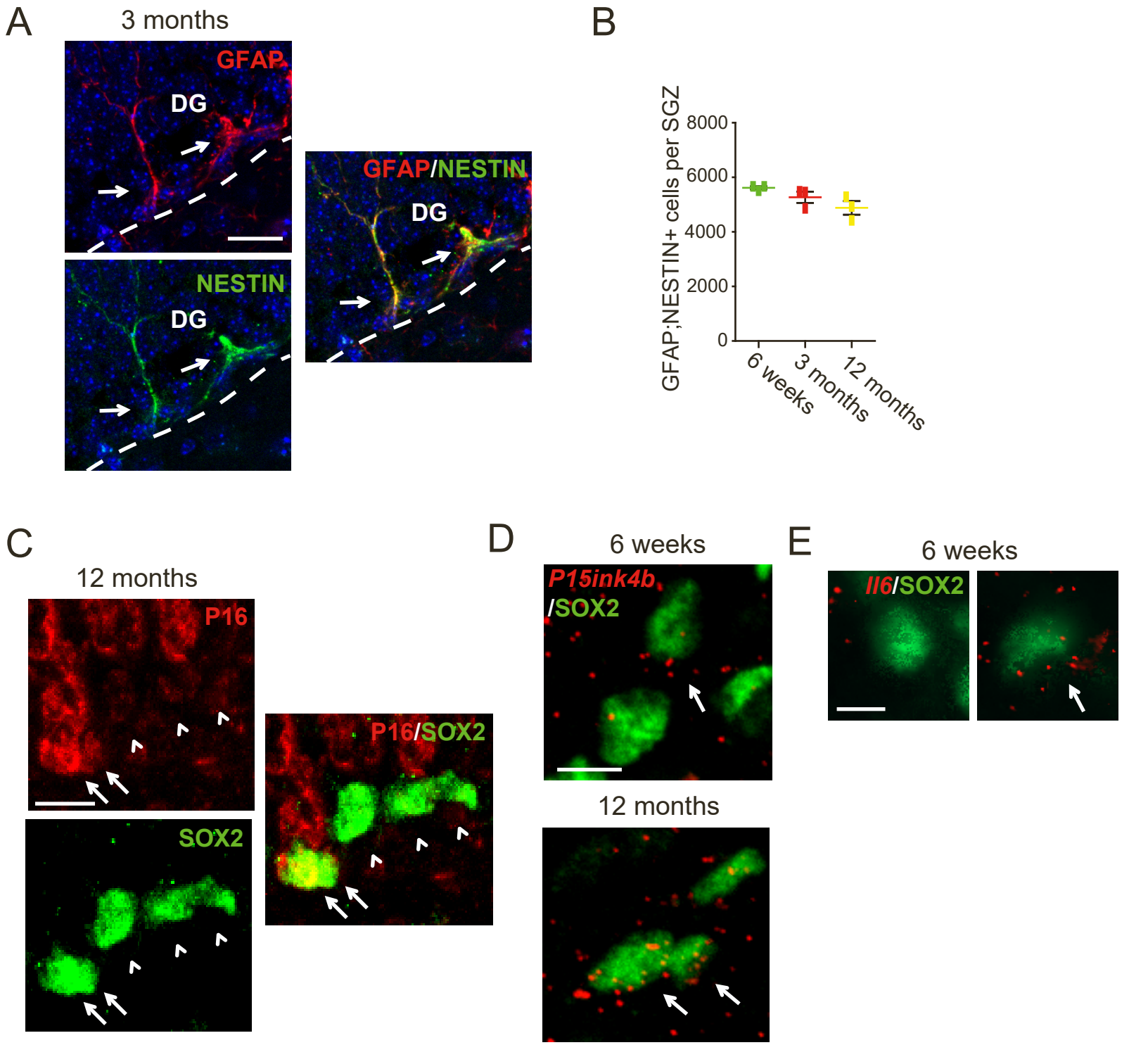
A
3 months
GFAP
DG
NESTIN
DG
GFAP/NESTIN
DG
B
GFAP;NESTIN+ cells per SGZ
8000
6000
4000
2000
0
6 weeks
3 months
12 months
C
12 months
P16
SOX2
P16/SOX2
D
6 weeks
P15ink4b
/SOX2
12 months
E
6 weeks
Il6/SOX2

Figure S1: ***Senescent NPCs accumulate in the SGZ with age, while neural stem cell numbers are unchanged.*** **Related to Figures 1 and 2.** Coronal sections through the hippocampal dentate gyrus (DG) of mice 6 weeks, 3 months, and 12 months of age were analyzed by immunostaining and FISH. (A) Image of the dentate gyrus from a mouse aged 3 months immunostained for GFAP (red) and NESTIN (green), counterstained for Hoechst 33258 (blue). Arrows denote double positive cells, and the dashed line indicates the boundary of the SGZ with the hilus. Scale bar = 20μm. (B) Quantification of sections as in (A) for the total number of GFAP;NESTIN double-positive cells in the dentate gyrus. n = 3 mice per timepoint. (C) Representative images of the SGZ from a mouse aged 12 months immunostained for p16 (red) and SOX2 (green). Arrows denote P16-positive, SOX2-positive cells, while arrowheads indicate SOX2-positive P16-negative cells. Scale bar = 10μm. (D) Representative images from the SGZ of 6 week and 12 month old mice analyzed by combined immunostaining for SOX2 (green) and FISH for *P15ink4b* (red). Arrows indicate cells positive for both SOX2 and *P15ink4b*. Scale bar = 10μm. (E) Images of the SGZ of a 6 week old mouse analyzed by combined immunostaining for SOX2 (green) and FISH for *Il6* (red) showing a SOX2-positive cell that is negative for *Il6* (left panel) and a SOX2-positive, *Il6*-positive cell (right panel, arrow). Scale bar = 5μm. In all cases, error bars indicate standard error of the mean.

A

Vehicle

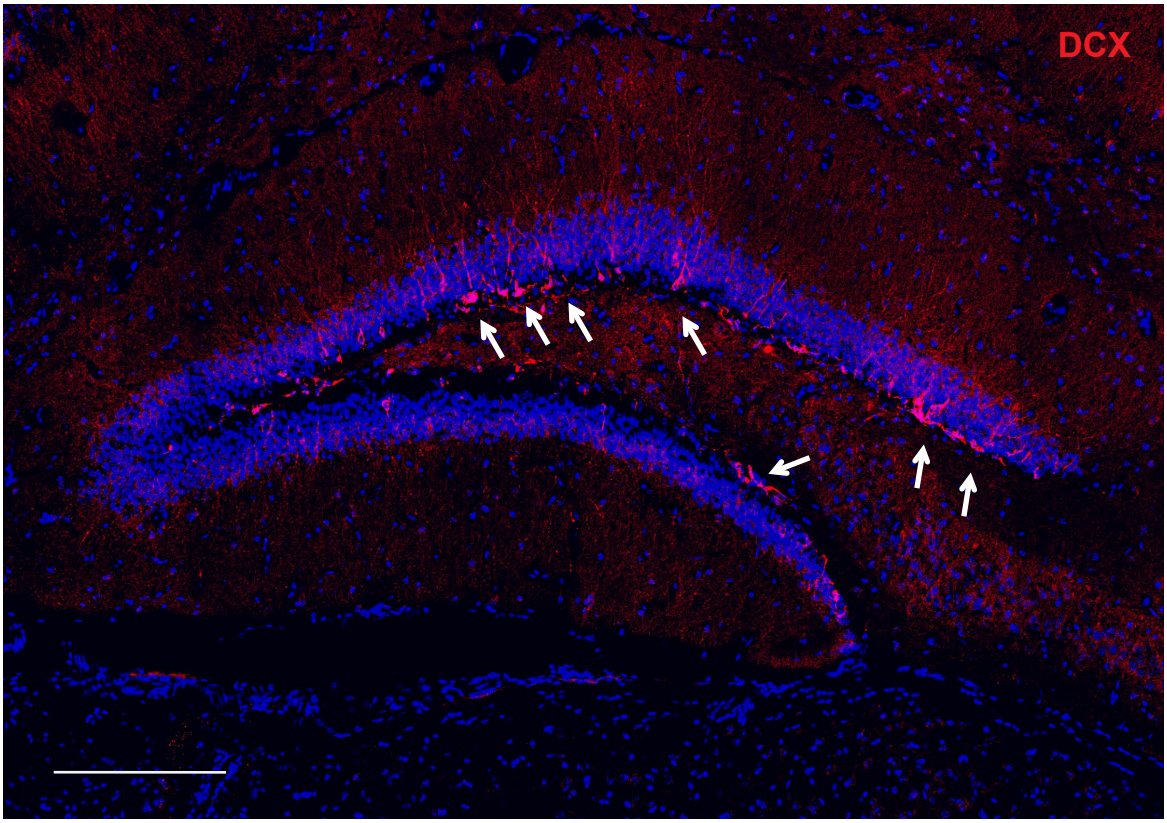

ABT263

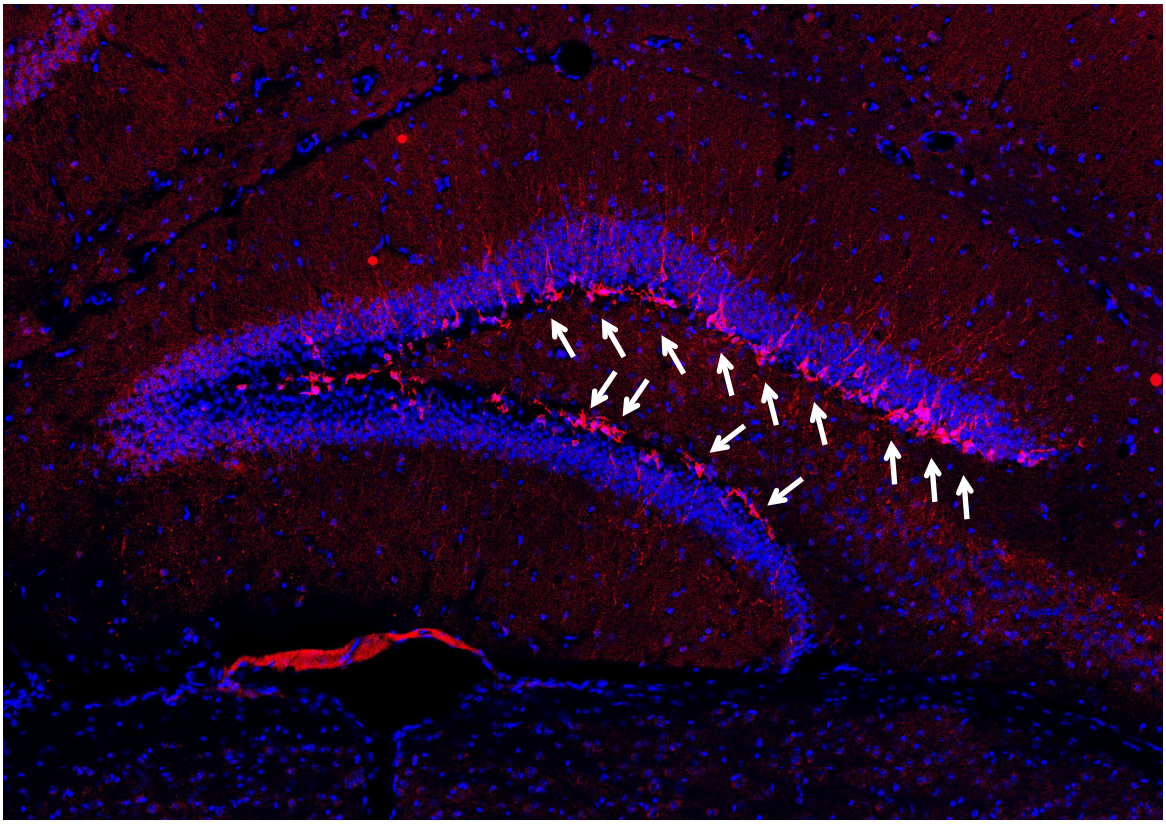

Figure S2: ***ABT-263 treatment enhances hippocampal neurogenesis in 3 month old mice.*** **Related to Figure 4.** Stitched images of coronal sections showing the dentate gyrus of 3 month old mice injected 5 days previously with either vehicle or ABT-263, immunostained for DOUBLECORTIN (DCX, red) and counterstained with Hoechst 33258 (blue). Arrows denote positive cells. Scale bar = 200 μm.

Supplemental Experimental Procedures

Neuroanatomy and Immunostaining: Mice were sacrificed by an overdose of sodium pentobarbital, and then transcardially perfused with PBS followed by 4% paraformaldehyde. Brains were post-fixed overnight in 4% paraformaldehyde, dehydrated in 30% sucrose-PBS, cryoprotected, and coronally sectioned at 20μm using a Leica CM 1850 cryostat (Leica Biosystems, Concord, ON, Canada). Immunostaining was performed as described previously (Cancino et al., 2013) and in detail in the Supplemental Methods. SA-*β*-Gal staining was performed using the Senescence β-Galactosidase Staining Kit (9860, Cell Signaling Technology, Danvers MA, USA) following the manufacturer's instructions. To combine with immunostaining, sections were first stained with SA-*β*-Gal, permeabilized, blocked and incubated with primary antibody as above. Secondary antibody labelling and Diaminobenzidine (DAB) staining were performed using the Rabbit specific HRP/DAB (ABC) Detection IHC Kit (Ab64261, Abcam, Cambridge, MA, USA) according to the manufacturer's instructions. Sections were washed with TBS, permeabilized with 0.4% Triton X-100 in TBS, and blocked with 5% BSA, 0.4% Triton X-100 in TBS. Slides were then incubated overnight at 4 °C with primary antibody diluted in blocking solution. Slides were washed with TBS, incubated with secondary antibody in blocking solution for 1 hour at room temperature, and mounted with Permount solution (Thermo Fisher Scientific, Waltham, MA, USA). For immunostaining of cultured cells, cells were fixed with 4% PFA or 2% formaldehyde/0.2%glutaraldehyde, blocked, and permeabilized with 10% normal goat serum (NGS) and 0.3% Triton-X. Fixed cells were then incubated with primary antibodies at 4ºC overnight, with secondary antibodies at room temperature for 1 hour, counterstained with Hoechst 33258.

Antibodies: The following antibodies were used for the immunofluorescent and western blot experiments in this study: goat anti-SOX2 (Y-17, 1 : 500, Santa Cruz Biotechnology, Santa Cruz, CA, USA), goat anti-DOUBLECORTIN (C-18, 1 : 250, Santa Cruz Biotechnology), rat anti-BrdU (OBT0030, 1 : 200, ABD Serotec, Raliegh, NC, USA), AlexaFluor 555-conjugated mouse anti-NeuN (MAB377A5, 1 : 100, EMD Millipore), mouse anti-KI67 (556003, 1 : 200, BD Pharmingen, San Diego, CA, USA), mouse anti-P16 (F-12, 1 : 1000, Santa Cruz Biotechnology), mouse anti-*γ*H2AX (05–636, 1 : 250, EMD Millipore), rabbit anti-GFAP (Z0334, 1 : 1000, Dako, Santa Clara, CA, USA), mouse anti-GFAP (A21282, 1 : 1000, Life Technologies, Grand Island, NY, USA), mouse anti-ASCLI1/MASH1 (556604, 1 : 1000, BD Pharmingen), rabbit anti-LAMIN B1 (AB16048, 1 : 500, Abcam), rabbit anti-IBA1 (019-19741, 1 : 500, Wako), rabbit anti-DOUBLECORTIN (AB18723, 1 : 500, Abcam), mouse anti-NESTIN (ab6142, 1:100, Abcam), rabbit anti-S100 (Z0311, 1 : 1000, Wako), and rabbit anti-ERK1 (K-23, 1:10 000, Santa Cruz Biotechnology). Secondary antibodies were AlexaFluor 488/555/647/HRP-conjugated donkey anti-goat, anti-rabbit, anti-rat, and anti-mouse IgG and anti-chicken IgY (1 : 1000, Life Technologies).

BrdU/EdU Labeling: For proliferation studies, mice were injected i.p. with a single dose of 100mg/kg BrdU (Sigma-Aldrich) or EdU (Thermo Fisher Scientific),and sacrificed and perfused as above 24 hours

later. To detect BrdU, coronal sections were incubated in 2N HCl for 30 minutes at 37°C, rinsed with TBS, incubated with anti-BrdU antibody at 4°C overnight, and detected using an anti-rat secondary antibody. To detect EdU, the Click-iT Plus EdU Alexa Fluor 555 Imaging Kit (C10638, Thermo Fisher Scientific) was used according to manufacturer's instructions. To label adult-born neurons, mice were injected i.p. with 100mg/kg BrdU every 2 hours for a total of 8 hours (5 injections) and sacrificed 30 days later. The day following BrdU immunostaining, sections were incubated with AlexaFluor 555 conjugated anti-NeuN antibody for 1 hour at room temperature. In both cases, labelled cell numbers were determined as described below. For olfactory neurogenesis, olfactory bulbs were sectioned at 18µm and 10 sections, sampled every 10th section, were immunostained for BrdU and NeuN, as described above.

Single molecule Fluorescence In Situ Hybridization (FISH): Single molecule FISH experiments were performed using the RNAScope® Multiplex Fluorescent Assay kit (Bio-techne, Minneapolis, MN, USA) according to the manufacturer's instructions. Briefly, 20µm brain sections were dehydrated with ethanol, pretreated with protease, and probe hybridization and signal amplification performed. Sections were then washed with TBS and immunohistochemistry was performed as above. Positive signals were identified as punctate dots present in the nucleus and/or cytoplasm. Z stacks were obtained through the entire thickness of the section, and in some cases the number of RNA granules per cell was quantified. The following probes were used: *Cdkn2b* (458341, Bio-techne), and *Il6* (315891, Bio-techne).

Neurosphere Assay: For adult cultures, the V-SVZ of the lateral ventricles was dissected out as previously described (Fujitani et al., 2010). Cell density and viability were determined using trypan blue exclusion and a hemocytometer. Freshly isolated cells were then plated at a density of 10 cells/µl in six-well (2 ml per well) ultra-low attachment plates (Corning, Corning, NY, USA) in serum-free medium containing 20ng/ml EGF (Sigma-Aldrich), 10ng/ml FGF2 (Sigma-Aldrich), and 2µg/ml heparin (Sigma-Aldrich). Primary neurospheres were mechanically dissociated, passed through a 40-µm cell strainer, plated at a density of 2 cells/µl. To induce senescence, secondary neurospheres were grown for 2 days, treated with 25nM Camptothecin (Sigma-Aldrich) for 72 hours, washed, and then replated in fresh medium for an additional 2 days. DMSO was used as a vehicle control for all drug treatment experiments.

Quantitative PCR: RNA was extracted from tissue or cultured cells using the E.Z.N.A. Total RNA Kit I and was treated with DNase I. cDNA was synthesized from 200ng total RNA, and quantitative PCR was performed. *Gapdh* mRNA was used as an internal control for all reactions, and all reactions were run in triplicate. Quantitative PCRs were run on C1000 Touch Thermal Cycler (Bio-Rad, Hercules, CA, USA), and analyzed using Bio-Rad CFX Manager Software (Bio-Rad). The following primers were used to for QPCR analysis: *mRFP* (Nam et al., 2007; Forward:CCAAGCTGAAGGTGACCAAG, Reverse: TCAAGTAGTCGGGGATGTCG), *Adam10* (Murthy et al., 2012; Forward: GATGCCAACCAGCCAGAGGG, Reverse: CAGATGCTGGGCAAAGGGCT), *Adam17* (Murthy et al.,

2012; Forward: CGGAGGAAGCAGGCTCTG, Reverse: GTTTCTAAGTGTGTCGCAGACTG), *Gapdh* (Forward: GGGTGTGAACCACGAGAAATA, Reverse: CTGTGGTCATGAGCCCTTC), and *Mmp2* (Forward: TAACCTGGATCCCGTCGT, Reverse: TTCAGGTAATAAGCACCCTTGAA). *Il6* transcript was detected using PrimePCR SYBR Green Assay primers (qMmuCED0045760) obtained from Bio-Rad.

Western Blot Analysis: Western blots were performed as described previously (Fatt et al., 2014). Briefly, secondary neurospheres were treated with either DMSO or camptothecin (as described above) and were collected via centrifugation. Samples were lysed in Radioimmunoprecipitation assay buffer (RIPA) supplemented with Aprotinin, Leupeptin, PMSF, Sodium Fluoride, and Sodium Orthovanadate. For each sample, 20mg of protein were loaded and run on a 15% SDS-PAGE gel. Following PAGE, the samples were then transferred to a 0.2-mm nitrocellulose membrane, blocked for 30 min with 5% BSA, 0.1%Tween-20 in TBS, and incubated overnight at 4 ˚C with primary antibody in blocking buffer. After several washes with 0.1%Tween-20 in TBS, membranes were incubated with secondary antibody at room temperature for 1 h. After several more washes, immunolabelling was detected via chemiluminescence.

Mini-Pump Implantation and ICV Injections: Mice were pre-treated with atropine sulfate (0.1mg/kg, ip), anesthetized (chloral hydrate, 400mg/kg, ip) and placed in a stereotaxic frame. Osmotic Minipumps (Model 1007D and Brain Infusion Kit 000851, Alzet Osmotic Pumps, Cupertino CA, USA) were implanted at the following coordinates – AP -0.5, ML -1.1, DV -2.0. The minipump was filled with the GCV (2.5mg/mL) or PBS and subcutaneously inserted for 7 days. All mice were treated with analgesia (ketoprofen, 5mg/kg, sc) following surgery. For ICV injections, mice were anesthetized and placed in a stereotaxic frame. Intracerebroventricular (ICV, coordinates: AP -0.5, ML -1.1, DV -2.5) microinjections of the ABT-263 or vehicle were performed (1ul/side, 0.12ul/minute) via glass micropipettes connected via polyethelene tubing to a microsyringe (Hamilton, Reno, NV). Micropipettes remained in place for 5 minutes after microinjection to ensure drug diffusion.

Quantification: Positive cell numbers in stained sections were quantified either by direct counts on the microscope or by counting cells in images captured using either Axiovision or Zen software (Zeiss, Oberkochen, Germany) on a Zeiss Axioplan 2 microscope with a Hamamatsu (Bridgewater, NJ, USA) Orca-R2 CCD camera, or with Volocity software (Perkin-Elmer, Waltham, MA, USA) on an Olympus (Center Valley, PA, USA) IX81F-3 confocal microscope with a Hamamatsu EM-CCD camera. Similar results were obtained with both approaches. To obtain total relative numbers of stained cells within the dentate gyrus, the entire hippocampus was sectioned, and all positive cells were counted in 10 sections, sampled every tenth section, after staining. The number of positive cells was then multiplied by 10 (to compensate for sampling frequency) to obtain the total relative number of positive cells in the dentate gyrus. To obtain the proportion of double-labeled cells, all single- and double-labeled cells were counted

in 10 sections spanning the entirety of the hippocampus. The SGZ was defined as the two cell layers beneath the granular cell layer of the hippocampus. Analyses of the lateral ventricle were performed in a similar manner to those described above for the hippocampus. For analysis of FISH, Z-stack images were taken from random regions of the SGZ and the number of punctate dots per cell was quantified from at least 200 Sox2-positive cells per animal. For *P15ink4a* mRNA, cells with at least 6 punctate dots were counted as positive while for *Il6* mRNA, cells with at least 2 dots were counted as positive.

Water Maze Training and Test Probes: Mice were trained in the hidden platform version of the water maze. A circular pool (120cm diameter, 50cm height) was filled with water (28^{o}C) to a depth of 40cm. Water was made opaque by the addition of nontoxic paint. A circular escape platform (10cm diameter) was submerged approximately 0.5cm below the surface of the water in the centre of one of the pool quadrants (N, S, E, W). The pool was surrounded by a curtain painted with 5 large, distinct geometric shapes located 1–1.5m from the pool wall. Mice received 3 consecutive block-training trials per day for 6 consecutive days. Each trial began by placing the mouse into the pool, facing the wall, from one of four possible start positions. The order of the release points varied pseudorandomly across days. The trial ended when the mouse reached the hidden escape platform or after 60 seconds had elapsed. If the mouse failed to locate the hidden platform, the experimenter's hand was placed over the platform (to serve as a visual cue) and the mouse was given an additional 15 seconds to find the platform. If the mouse failed to do so, it was gently guided to the platform. The mouse stayed on the platform for 15 seconds after which it was placed on a heated blanket for an additional 15 seconds (total inter-trial interval of approximately 30 seconds). Memory was tested using a probe test 24 hours following the last training session. During the probe test, the escape platform was removed from the water and the mouse was allowed to swim freely for 60 seconds. The mouse's behavior in the pool was recorded by an overhead video camera and tracked using automated software (Watermaze 3.0, Actimetrics). During training, we analyzed escape latency, distance travelled, and swim speed. In the probe test, we quantified spatial memory by measuring amount of time mice spent searching in the target zone (20cm radius, centered on location of platform during training, corresponding to 11% of pool surface) versus average time spent in three other equivalent zones in other areas of pool (Moser et al, 1998).

Contact for Reagent and Resource Sharing

Further information and requests for resources and reagents should be directed to and will be fulfilled by the Lead Contact, David R. Kaplan (dkaplan@sickkids.ca).

Supplemental References

Cancino, G.I., Yiu, A.P., Fatt, M.P., Dugani, C.B., Flores, E.R., Frankland, P.W., Josselyn, S.A., Miller, F.D., Kaplan, D.R., 2013. p63 regulates adult neural precursor and newly born neuron survival to control hippocampal-dependent behavior. J. Neurosci. 33, 12569–12585.